Computation Methods for Parametric Analysis of Gravitational Wave Data

Heta A. Patel

Thesis submitted to the Faculty of the

Virginia Polytechnic Institute and State University

in partial fulfillment of the requirements for the degree of

Master of Science

in

Electrical Engineering

J. Michael Ruohoniemi, Co-chair

Lydia Patton, Co-chair

A. A. (Louis) Beex

August 13, 2019

Blacksburg, Virginia

Keywords: parameterized post-Einsteinian, ChirpLab, gravitational wave astronomy

Copyright 2019, Heta A. Patel

Computation Methods for Parametric Analysis of Gravitational Wave Data

Heta A. Patel

(ABSTRACT)

Gravitational waves are detected, analyzed and matched filtered based on an approximation of General Relativity called the Post Newtonian theory. This approximation method is based on the assumption that there is a weak gravity field both inside and around the body. However, scientists cannot justify why Post-Newtonian theory (meant for weak fields) works so well with strong fields of black hole mergers when it really should have failed [66]. Yunes and Pretorius [69] gave another approach called parameterized post-Einsteinian (ppE) theory that uses negligible assumptions and promises to identify any deviation on the parameters through post-processing tests. This thesis project proposes to develop a method for the parametric[1] detection and testing of gravitational waves by computation of ppE for the inspiral phase using ChirpLab. A set of templates will be generated with ppE parameters that can be used for the testing.

[1]Yunes and Pretorius [69] refer to theoretical assumptions and the deviation (in estimating the parameters) caused due to theory-dependence, as the 'fundamental theoretical bias' or simply 'bias'. The term 'bias' can be misinterpreted as a physical difference between the waveforms or the models, as was pointed out by my advisor. Hence, we will refrain from using the terminology used by Yunes and Pretorius [69] and instead use the term *deviation* in place of bias and *parametric* in place of unbiased.

Computation Methods for Parametric Analysis of Gravitational Wave Data

Heta A. Patel

(GENERAL AUDIENCE ABSTRACT)

Electromagnetic waves were discovered in the 19th century and have changed our lives with various applications. Similarly, this new set of waves, gravitational waves, will potentially alter our perspective of the universe. Gravitational waves can help us understand space, time and energy from a new and deeper perspective. Gravitational waves and black holes are among the trending topics in physics at the moment, especially with the recent release of the first image of a black hole in history. The existence of black holes was predicted a century ago by Einstein in the well defined theory, "Theory of General Relativity". Current approaches model the chaotic phenomenon of a black hole pair merger by the use of approximation methods. However, scientists Yunes and Pretorius [69] argue that the approximations employed skew the estimation of the physical features of the black hole system. Hence, there is a need to approach this problem with methods that don't make specific assumptions about the system itself. This thesis project proposes to develop a computational method for the parametric[2] detection and testing of gravitational waves.

[2]Yunes and Pretorius [69] refer to theoretical assumptions and the deviation (in estimating the parameters) caused due to theory-dependence, as the 'fundamental theoretical bias' or simply 'bias'. The term 'bias' can be misinterpreted as a physical difference between the waveforms or the models, as was pointed out by my advisor. Hence, we will refrain from using the terminology used by Yunes and Pretorius [69] and instead use the term *deviation* in place of bias and *parametric* in place of unbiased.

Acknowledgments

I would like to thank my advisor Dr. Patton, for introducing me to this topic. For her patience, guidance and encouragement through this whole process.

Dr. Ruohoniemi and Dr. Beex, for serving on my committee and their invaluable suggestions regarding this thesis.

Dr. Candes, for making the ChirpLab Software available to me and my research group. Dr. Pretorius, Dr. Yunes and Dr. Cornish for pointing me in the right direction.

Lastly, I would like to thank my parents (Ajay Patel and Smruti Patel) and brother (Hetul Patel) for always believing in me and my dreams.

This research has made use of data, software and/or web tools obtained from the Gravitational Wave Open Science Center (https://www.gw-openscience.org), a service of LIGO Laboratory, the LIGO Scientific Collaboration and the Virgo Collaboration. LIGO is funded by the U.S. National Science Foundation. Virgo is funded by the French Centre National de Recherche Scientifique (CNRS), the Italian Istituto Nazionale della Fisica Nucleare (INFN) and the Dutch Nikhef, with contributions by Polish and Hungarian institutes.

Lastly, I thank Advanced Research Computing at Virginia Tech for providing computational resources and technical support that have contributed to the results reported within this thesis. URL: http://www.arc.vt.edu.

Contents

List of Figures ix

List of Tables xii

1 Background 1

1.1 Introduction . . . 1

1.2 Motivation . . . 1

1.2.1 History of LIGO . . . 1

1.2.2 Purpose of this thesis . . . 2

1.3 Gravitational waves . . . 3

1.3.1 Types of gravitational waves . . . 4

1.4 Detection of GW . . . 5

1.4.1 Ground-based Detectors . . . 5

1.4.2 Infrastructure . . . 6

1.4.3 Detection of gravitational waves . . . 7

1.4.4 Matched filtering . . . 8

1.5 Outline . . . 8

1.6 Summary of the chapter . . . 9

2 Detection using extended ChirpLab **11**

2.1 Introduction . . . 11

2.1.1 CBC: chirp signal . . . 12

2.2 ChirpLab Statistics . . . 15

2.2.1 Chirplet Graph . . . 15

2.2.2 Likelihood Ratio . . . 18

2.2.3 Best Path Statistics . . . 19

2.3 Summary of the chapter . . . 21

3 Parameterized Post-Einsteinian Testing **22**

3.1 Introduction . . . 22

3.1.1 Classical tests . . . 23

3.2 Testing of Gravitational waves . . . 24

3.2.1 Parameterized Post-Newtonian Formalism . . . 25

3.2.2 Parameterized Post-Einsteinian Formalism . . . 28

3.3 Summary of the chapter . . . 30

4 Computational methods **31**

4.1 Introduction . . . 31

4.2 Current methods . . . 32

4.2.1 PyCBC . . . 32

4.2.2 LALsuite: IMRPhenomD . . . 33
4.3 ChirpLab with ppE . . . 33
4.4 Brans-Dicke . . . 35
4.5 Massive gravity . . . 36
4.6 Summary of the chapter . . . 37

5 Results **38**

5.1 Preliminary discussion . . . 38
5.2 Signal generation . . . 39
5.2.1 Inspiral: General Relativity . . . 40
5.2.2 Inspiral: Alternate theories . . . 41
5.3 Detection of GW using ChirpLab . . . 45
5.3.1 Best path: GR . . . 46
5.3.2 Best path: ppE . . . 47
5.4 Non-template based search on Real data . . . 49
5.5 Summary of the chapter . . . 52

6 Concluding remarks **53**

6.1 Conclusion . . . 53
6.2 Future work . . . 54

Bibliography **55**

Appendices **65**

Appendix A Description of $\tilde{h}_{gr}(f)$ **66**

List of Figures

1.1 An object expands and contracts with the passing of gravitational waves with polarization plus (top) and cross (bottom) *source:*[36]. 3

1.2 Aerial view of Livingston (left) [4] and Hanford (right) [5] LIGO interferometer sites. 6

1.3 Basic representation of Michelson interferometer with Fabry-Perot cavity [6] 7

2.1 Strain data on H1 detector for GW150914 event. The inset images show models of the CBC stages as the black holes coalesce. *Note: The waveform shown here are a reconstruction of the actual event.* [10, 29] 13

2.2 Illustration of CBC inspiral waveform with time of coalescence $t_c = 40s$. (Top plot) Signal represented in logarithmic scale shows the waveform as a shaded object. (Bottom plot) Last 5 milliseconds of the same signal. Clearly shows the sinusoidal oscillations before coalescing. [40]. 14

2.3 Illustration of a typical construction of graph using chirplets of variable length (as represented by the vertical lines) with the progression of time [25]. 16

2.4 Pictorial representation of line segments known as chirplets in the time-frequency plane (X-axis represents time, Y-axis represents frequency). ChirpLab uses a dictionary type structure of chirplets that is based on length, slope and vertex position offset [25]. 16

2.5 Validity of the successive chirplet in the chain of chirplets. Top Left: Valid continuation of the chain with minimal difference in slope **and** frequency offset at the juncture, Top Right: Unacceptable difference in slope, Bottom Left: Unacceptable vertex position offset and, Bottom Right: Unacceptable differences in slope and nonadjacent vertices [25]. 17

5.1 Signals generated using PyCBC a) GR chirp signal generated using PyCBC with IMRPhenomD, see [42]. b) GR chirp signal generated using PyCBC with TaylorT3 (Hulse-Taylor Binary, see [39]). 40

5.2 ppE waveform generated using ChirpLab. The signal approaches GR waveform with parameters $(\alpha, \beta, a, b) = (0, 0, a, b)$. a) GR chirp signal b) Beta value 41

5.3 Beta shown for Brans-Dicke and Massive gravity theories, a),b) shows the constrained value of β as per [69] c), d) shows unconstrained for visualization as per Table 4.1. 42

5.4 Waveforms are shown for Normal (PN), GR(PPE), Brans-Dicke(PPE) and Massive gravity (PPE) theories. a) Waveforms generated using constrained values of β b) Zoomed plot for constrained waveforms c) Waveforms simulated using unconstrained values of β d) Zoomed plot for unconstrained waveform. 43

5.5 Zoomed in 5.4 part c) 44

5.6 Frequency response of ppE generated waveforms 'GR', 'BD' and 'MG'. Freq Spectrum with a) constrained β b) unconstrained β. 45

5.7 a) Noise generated from PSD b) Best path with no signal present with number of chirplets=8. 46

5.8 Best path statistic (red thick line) for GR waveform. a) i) Inspiral signal generated using GR with masses=1.4, 1.4 and coalescing at $t_c = 0.25s$ ii) Instantaneous frequency shows the peak at the coalescence iii) PSD for noise with respect to frequency. b) Best path statistic for four subplots with number of chirplets=1,2,4, and 8 respectively. X-axis represents time in number of samples (s*Fs), Y-axis represents the Frequency (Hz). 47

5.9 ppE waveform approaches BD waveform with parameters as listed in Table 4.1. a) BD chirp signal generated using ppE. b) Best path statistic for chirplets length=1,2,4,8. 48

5.10 ppE waveform approaches MG waveform with parameters as listed in Table 4.1. a) MG chirp signal generated using ppE. b) Best path statistic for chirplets length=1,2,4,8. 49

5.11 Best path plots are shown for 3 different segments of real data using 8 multiscale chirplets. X-axis represents time in number of samples (s*Fs), Y-axis represents the Frequency (Hz). a) GPS 1126088704 b) 1128669184 c) 1186300472 or GW170809 is a confident detection in GWTC-1 catalogue d) Sample strain data of full 4096 seconds. 51

List of Tables

3.1 PPN parameters with the established constraints [66] 27

3.2 Values for ppE parameters 29

4.1 Values used for the calculation of β (constituting parameters) 36

List of Abbreviations

aLIGO Advanced Laser Interferometer Gravitational-waves Observatory

ARC Advanced Computing Research

BBH Binary Black Hole

BD Brans-Dicke

BH Black Hole

BP Best Path

CBC Compact Binary Coalescence

EFE Einstein's Field Equation

EOB Effective-one-body

GLRT Generalized Likelihood Ratio Test

GR General Relativity

GW Gravitational Wave

IMR Inspiral-Merger-Ringdown

ISCO Inner-most Stable Circular Orbit

LIGO Laser Interferometer Gravitational-waves Observatory

MG Massive Gravity

NR Numerical Relativity

NS Neutron Star

PN Post-Newton

ppE Parameterized Post-Einsteinian

PPN Parameterized Post-Newtonian

Chapter 1

Background

1.1 Introduction

In this chapter, we provide an overview of fundamental gravitational wave astronomy. The chapter begins with the description of gravitational waves and how they are generated, followed by the types of gravitational waves and the measurement techniques employed for ground-based detectors. In the end, we mention a signal processing technique used for gravitational wave analysis called matched filtering. Matched filtering is a well-known process in signal processing and is an optimal technique for extracting signal hidden in the noise. The information provided here will be instrumental (to readers new to the field) for understanding the basics of gravitational wave astronomy and the thesis. We recommend the readers to study the following sources for simple and informative description of the mathematical and physical concepts involved in Einstein's theory of General Relativity: d'Inverno [31], Maggiore [47], Misner et al. [49].

1.2 Motivation

1.2.1 History of LIGO

Einstein anticipated the existence of gravitational waves but considered these waves to be too weak to be detected. However, with technological advancements and increasing understanding of the universe, it became

possible. In the 1960s, Joseph Weber and Rainer Weiss independently proposed laser interferometry methods for detection of gravitational waves. Kip Thorne, in 1968, created a research group at Caltech aimed at design and operation of advanced gravitational wave interferometers. The National Science Foundation (NSF) funded Caltech and MIT research groups in 1980, led by Ronald Drever and Rainer Weiss, to conduct research and potentially build an interferometeric detector several kilometers long. As a result, Laser Interferometer Gravitational wave Observatory (LIGO) was founded in 1984 under the supervision of Drever, Weiss, and Thorne. Construction began on chosen sites in Hanford, WA and Livingston, LA. Initial LIGO detectors were operational from 2002 to 2010. Initial LIGO failed to detect any gravitational waves and hence, plans were made to build improved and more sensitive detectors called Advanced LIGO (aLIGO). Within just two days of operation, aLIGO detected the first gravitational wave on 14th Sept'15 with signal-to-noise ratio (SNR) of 24 on both detectors. aLIGO has so far detected 11 CBC gravitational waves, as listed in [2]. For the timeline of LIGO, see [8].

1.2.2 Purpose of this thesis

The principal purpose is to explore an analysis pipeline free of theoretical assumptions[1] for gravitational wave astronomy allowing for the signal to deviate from General Relativity. This thesis aims to incorporate parameterized post-Einsteinian (developed by Yunes and Pretorius [69] testing with a non-template[2] based detection method using a software package called ChirpLab (developed by Candes [24]). Current methods involve template-based matched filtering[3] searches for detection. These searches are computationally ex-

[1] Yunes and Pretorius [69] refer to theoretical assumptions and the deviation (in estimating the parameters) caused due to theory-dependence, as the 'fundamental theoretical bias' or simply 'bias'. The term 'bias' can be misinterpreted as a physical difference between the waveforms or the models, as was pointed out by my advisor. Hence, we will refrain from using the terminology used by Yunes and Pretorius [69] and instead use the term *deviation* in place of bias.

[2] Here 'template' refers to GR theory-based simulation of gravitational waves. The term does not indicate the general interpretation of the word.

[3] optimal filter used to detect known signals, described in Section 1.4.4

pensive[4]. ChirpLab has been demonstrated to significantly lower computational cost for initial searches. The methods purposed in this thesis also allow for computational post-data analysis using a parameterized post-Einsteinian framework, a growing research program which contributes to rigorous testing of the theory of general relativity.

1.3 Gravitational waves

Einstein's theory predicted that massive accelerating bodies produce distortion of spacetime in the form of gravitational waves (GWs). Einstein revamped Newton's theory of gravity by arguing that gravity was an acceleration that changes how spacetime behaves around a mass. When a GW passes through spacetime, it distorts the spacetime fabric and any massive object in its path will wobble, as shown in Figure 1.1.

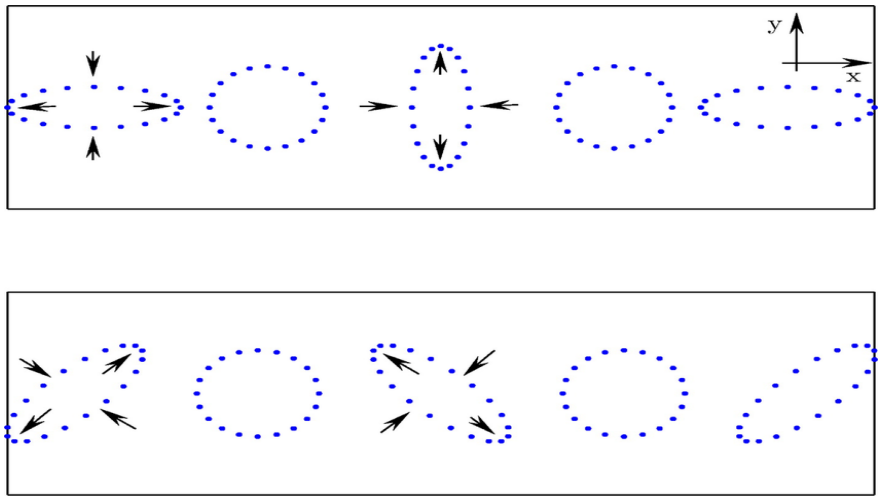

Figure 1.1: An object expands and contracts with the passing of gravitational waves with polarization plus (top) and cross (bottom) *source:*[36].

Depending on the polarization of the wave, the object would appear to expand or compress along certain directions of polarization. The wave would also seemingly slow down the passage of time[5] for an observer

[4]According to Owen and Sathyaprakash [51], aLIGO requires $8 * 10^{-11}$ flop (floating-point operations per second) to compute single step matched filtering.

[5]Note that according to Einstein, time and space are not considered a separate object but instead defined

in the path of the GW. Both length contraction and time dilation are observed phenomena and follow the Lorentz transformation [57].

1.3.1 Types of gravitational waves

Every object generates gravitational waves, but only the ones produced by massive objects will be strong enough for current detectors. The scientists have defined four types of GWs depending on the sources. For our current ground-based detectors, the most likely sources are the coalescence of black holes or neutron stars. Each type of wave has a unique signature that the Laser Interferometer Gravitational-Wave Observatory (LIGO) and Virgo detectors can identify.

Continuous GW

Any moving (with non-zero acceleration) object generates gravitational waves. Massive, spinning, singular objects like neutron stars produce continuous gravitational waves. The signal varies slowly in amplitude and frequency, hence the name 'continuous'. Researchers have simulated audio of these waves, see [46].

Stochastic GW

Numerous tiny waves may be observed simultaneously, and thus must be measured by superposing the waveforms of each wave upon each other. Scientists classify the combination of these waves as stochastic waves. These are the most difficult to model and detect; some fragments of a stochastic signal might even have originated from the big bang [7].

---

together as spacetime. This statement considers time as continued progress of existence.

Compact Binary Coalescence (CBC) GW

Waves generated as a result of coalescence of two massive objects (generally a spinning black hole (BH) or neutron star (NS) pair) are called Compact Binary Coalescence (CBC) GWs. CBC GWs are the most probable type of waves that the current instruments can detect. As a matter of fact, all 11 candidates detected by LIGO are CBC waves. The coalescence phenomenon is divided into three different phases: inspiral, merger, and ringdown, as explained in Chapter 2.1.

Burst GW

Burst waves generally correspond to GWs arising from gamma-ray bursts or supernova (that result in the birth of BH or NS). This type of wave is very difficult to model since the researchers do not know what to expect. Considering these waves occur with an unanticipated source, burst GWs are studied using unmodeled methods and filters. See [3].

1.4 Detection of GW

1.4.1 Ground-based Detectors

The first attempt to detect gravitational waves was made by Weber in 1960. He hoped to measure the vibration of aluminum cylinders and developed a resonant mass detector [53]. Current age detectors are based on interferometry, more precisely the instruments are Michelson interferometers with folded arms in the form of a Fabry-Perot cavity. As shown in Figure 1.2 there are two detectors in the USA, one in Livingston, LA and the other in Hanford, WA.

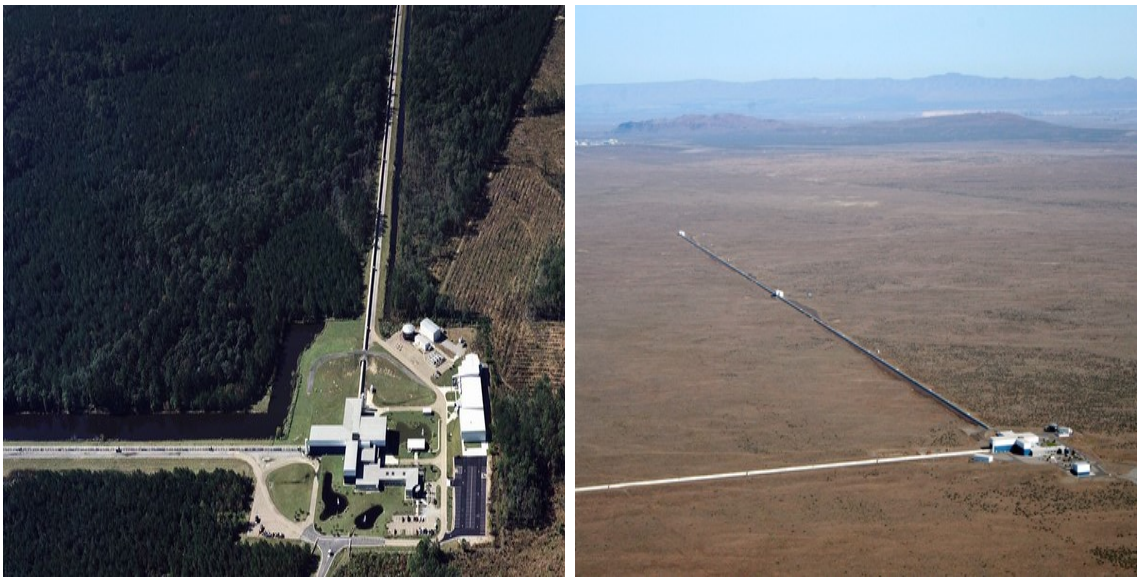

Figure 1.2: Aerial view of Livingston (left) [4] and Hanford (right) [5] LIGO interferometer sites.

1.4.2 Infrastructure

These detectors have two mirrors hanging by pendulums on each of the 4km long arms. The arms are "folded", two additional mirrors that keep reflecting to increase the length of an arm. The arms are equipped with Fabry-Perot cavities. Fabry-Perot cavities, the main improvement in Advanced LIGO (aLIGO), amplify the resonance of the wave in the cavity and create a standing wave [64]. The mirrors are kept in seismic isolation as environmental noise can make the detection impossible; the actuators feedback measures the ground vibration and counters it to make the 'mirrors float'. The isolation mechanism reduces noise up to six orders of magnitude. LIGO's recently upgraded devices are capable of measuring a change in the distance on the order of 10^{-22} m. Improving the sensitivity of the detectors is necessary for gravitational waves as the signal strength is very feeble and of 10^{-22} order of magnitude. aLIGO has improved upon the infrastructure by upgrading mirrors, suspension, and seismic isolation. More information can be found at [1].

1.4.3 Detection of gravitational waves

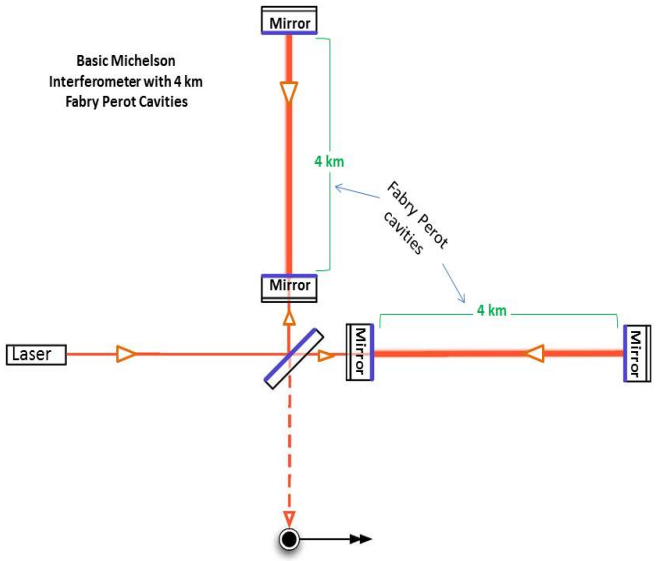

Figure 1.3: Basic representation of Michelson interferometer with Fabry-Perot cavity [6]

.

By the time a GW reaches Earth, the amount of spacetime distortion generated is thousands of times smaller than the size of an atomic nucleus. The interferometers used for detection of gravitational waves are among the most sensitive instruments in the world; measuring a distance of 10^{-22} m [7]. The basic design is modeled on the Michelson interferometer. A laser beam is radiated on a mirror, the principal beam is split into two beams, one is allowed to pass through and the other is reflected by 90 degrees as shown in Figure 1.3. A photodetector measures the light intensity of the reflected/recombined beam. In normal operation, where the length of both arms remains unchanged, the beams cancel each other out and nothing reaches the photodetector. When a GW passes through the detector, it will change the length of one arm and the laser light must travel further resulting in a brighter recombined beam. The signal observed at the photodetector is the *strain*[6] data later analyzed.

[6] a common terminology in GW physics representing the dimensionless amplitude 'strain', which is equal to twice of the observed displacement in the laser beam of the interferometer.

1.4.4 Matched filtering

As mentioned in Section 1.3.1, there are four types of GWs depending on the source. Each type of GW has a signature vibration pattern. For example, continuous GWs appear sinusoidal as the signal is slowly varying with amplitude and frequency. CBC GWs have wave structure of chirp signals with rapidly varying frequency as two massive objects coalesce within seconds. The CBC waves depend on various *parameters*, including the masses of the two objects, their spin, the orbital frequency of the two masses and so on. Matched filtering maximizes the signal-to-noise ratio to detect a signal subject to noise. The data is processed to remove noise (quantum or shot noise, environmental noise, and seismic noise) using optimal matched filtering techniques. Essentially, Matched filter measures the cross-correlation of the signal to a known waveform. Since the waveform is not entirely known and depends on the said parameters, a collection of all the simulated template waveforms is generated to cover the parameter space (from here on referred to as a template bank). These templates are used by the matched filter for the detection algorithm. The currently used software package, PyCBC, generates the template bank by varying the mass ratio and spins. The waveforms are simulated under the assumption that the dynamics of the system are correctly modeled using the linearized field equations of General Relativity (GR). The equations will be discussed in Section 3.2.1.

1.5 Outline

This thesis is organized in five chapters, the first chapter (1) being a brief review of gravitational waves and of the working principles of the LIGO interferometers. In chapter 2, a non-template based detection method using ChirpLab software are discussed. The introduction is followed by an explanation of the statistics involved in this detection method.

Chapter 3 introduces the reader to different frameworks for testing GR. The parameterized post-Einsteinian (ppE) framework aims to allow for the existence of plausible non-GR waves, as shown later in the chapter.

Chapter 4 discusses computational methods for the theories addressed in previous chapters. The chapter starts with an introduction to currently used computation methods, namely PyCBC and LALsuite (`lalsuite`). Our computation of ppE is discussed next.

The last chapter 5 starts with our simulated gravitational waves followed by our results from ppE computation. In the end, we test ChirpLab with the computed ppE waveforms. We also showcase the results from our search using ChirpLab on real aLIGO data for a recognized event and on an uneventful data segment from the O2 [7]observation run.

1.6 Summary of the chapter

In essence, this chapter gives the reader an idea about how gravitational waves are generated and the process for measuring gravitational waves. Gravitational waves distort the spacetime fabric with the passage. In effect, any object in the path of a gravitational wave expands and contracts. Such distortion of an object enables us to detect the gravitational waves through interferometry. We present an introduction to the LIGO detection mechanism using Michelson laser interferometer. Lastly, we discuss the currently used technique for detection and parameter estimation, namely matched filtering. Matched filtering is a process used to recover a known signal embedded in noise. However, the signal is not known in our case, and so current methods create a template bank (by varying different parameters to generate different waveforms) to cover the parameter space for all possible signals. It must be remembered that the templates are generated using linearized field equations of GR. This thesis questions the validity of such GR-dependent approaches. The following document advocates the need for a gravitational wave analysis pipeline independent of theoretical assumptions.

The first step for the pipeline is detecting the presence of a potential signal. We make use of the MATLAB package developed by Candes [24] for a non-template based detection algorithm. For post-processing pur-

[7]The second observing run for aLIGO started on 30 Nov'16 and ended on 25 Aug'17.

poses, we explore the Parameterized Post-Einsteinian (ppE) framework. The ppE theory was proposed by Yunes and Pretorius [69], to eliminate deviation[8] arising from currently used approaches. The ppE theory combines General Relativity (GR) and other competing theories by the use of ppE parameters. We extend the ChirpLab suite to incorporate ppE waveforms. As will be seen in Section 5.3, we have included ChirpLab detection results for ppE waveforms to showcase the effectiveness of both ChirpLab and ppE.

[8] Yunes and Pretorius [69] refer to theoretical assumptions and the deviation (in estimating the parameters) caused due to theory-dependence, as the 'fundamental theoretical bias' or simply 'bias'. The term 'bias' can be misinterpreted as a physical difference between the waveforms or the models, as was pointed out by my advisor. Hence, we will refrain from using the terminology used by Yunes and Pretorius [69] and instead use the term *deviation* in place of bias.

Chapter 2

Detection using extended ChirpLab

2.1 Introduction

Einstein predicted the behavior of massive accelerating bodies back in 1915 with the 'Theory of General Relativity'. One of his profound inferences was the existence of black holes and gravitational waves. The detection of gravitational waves in 2016, about 100 years later, became the most important discovery of that decade. Einstein's theory thoroughly models the dynamics of black holes and how black holes interact with spacetime. Kip S. Thorne is pleasantly amused by the extensiveness of the theory as expressed in his book 'The Science of Interstellar':

> If we know the mass of a black hole and how fast it spins, then from Einstein's relativistic laws we can deduce all the hole's other properties: its size, the strength of its gravitational pull, how much its event horizon is stretched outward near the equator by centrifugal forces, the details of the gravitational lensing of objects behind it. Everything. This is amazing. So different from everyday experience. It is as though knowing my weight and how fast I can run, you could deduce everything about me: the color of my eyes, the length of my nose, my IQ,.. [61].

Thorne mentions the ease with which we can infer system properties based on only a few fundamental parameters using Einstein's relativistic laws. However, the current analysis techniques neglect the possibility

of waves not following Einstein's relativistic laws exactly. The principal purpose of this thesis is to explore a parametric analysis pipeline for gravitational wave astronomy allowing for the observed GW to deviate from General Relativity. The coalescing binary black holes system proves to be the most promising source for detection of GWs, and hence we shall focus on signals from binary black hole (BBH) systems. The same method of analysis can also be applied to neutron stars and other massive astronomical bodies. This project focuses on the Compact Binary Coalescences type of GW, mergers of black holes. All 11 observations made by aLIGO are of this (CBC) type.

Here, we extend a non-template[1] based detection technique developed by Candes [24]. ChirpLab is a MATLAB software developed for detection of chirp signals. This is a generalized software and works for any type of chirp signal. The generic search approach is substantial as we are aiming to remove the dependency on the theoretical templates. The ChirpLab software does not depend on any theoretical assumptions and only uses statistical analysis for detection.

2.1.1 CBC: chirp signal

The coalescence phenomenon is divided into three stages, as illustrated in Figure 2.1: inspiral, merger and ringdown (IMR). Figure 2.1 also shows the progression of a GW signal with the physical stages of the phenomenon. The waveform shown here is the reconstruction of LIGO's first-ever detection of the event GW15019. The inspiral marks the beginning of the end of the binary system[2], which as a result will become a single massive astronomical body. The three stages are roughly described by Anderson and Balasubramanian [14] as:

- The inspiral component describes the evolution of the binary system up to the "innermost stable circular orbit" (ISCO). This component is well modeled for BBH systems of $\sim$

[1] Here 'template' refers to GR theory based simulation of gravitational waves. The term does not indicate the general interpretation of the word.

[2] A binary pair can consist of a combination of a black hole, neutron star, white dwarf star or any astronomical object generally.

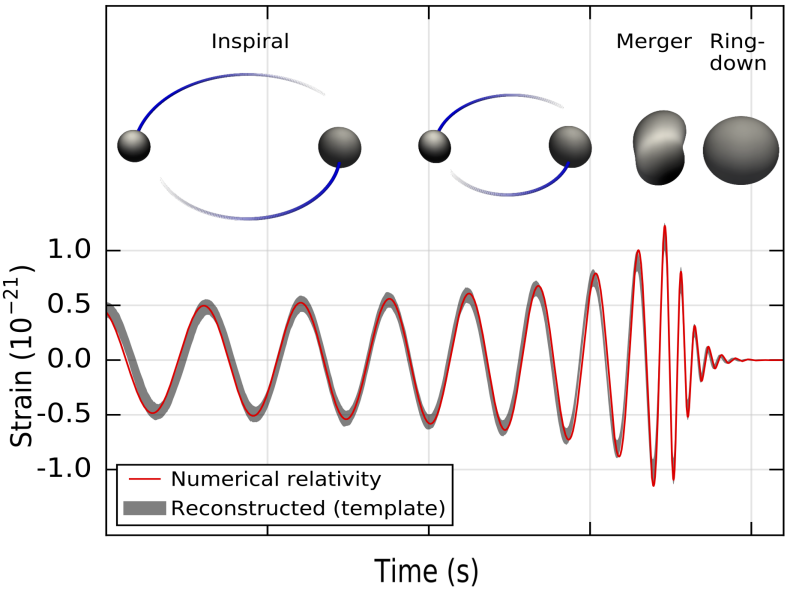

Figure 2.1: Strain data on H1 detector for GW150914 event. The inset images show models of the CBC stages as the black holes coalesce. *Note: The waveform shown here are a reconstruction of the actual event.* [10, 29]

$1M_{\odot}$[21], but there is some doubt whether it is known well enough for optimal filtering for binaries of total mass $\gtrsim 20M_{\odot}$.

- The merger component describes the evolution of the system from ISCO until such time as the system can be described as a single perturbed Kerr black hole. No analytical descriptions of this component exist.
- The quasi-normal ringdown component describes the evolution of the system when it is well described as a single perturbed Kerr black hole. This component is well modeled for all binary black hole coalescences (BBHC).

All the stages are studied with the Post-Newtonian (PN) approximation to solve Einstein's equations [26, 27]; or with Numerical Relativity (NR). NR is the only method to solve the entire equations including merger and ringdown [44]. The entire waveform can also be modelled with the binaries defined as essentially a single object, using the "Effective-one-body" (EOB) formalism [23, 52]. The idea is to transfer Einstein's

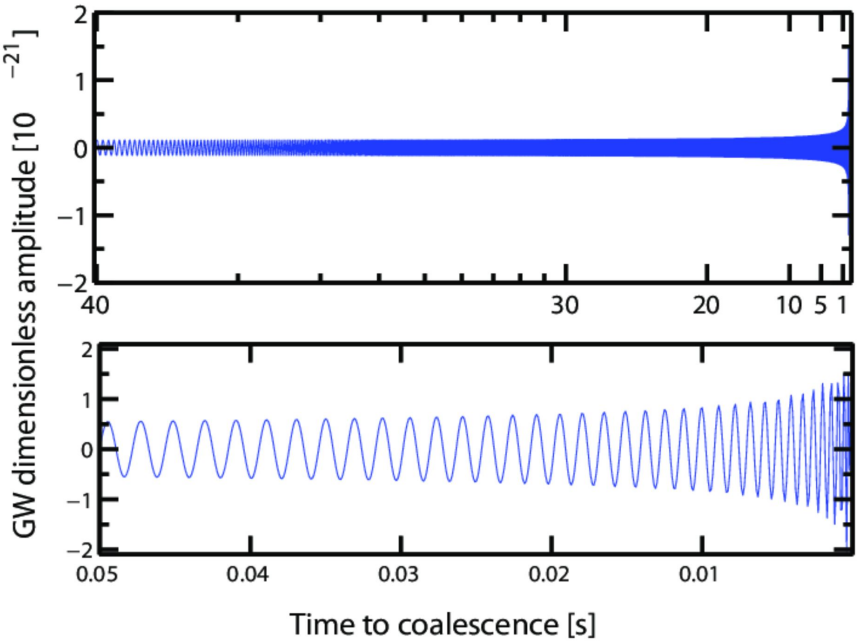

Figure 2.2: Illustration of CBC inspiral waveform with time of coalescence $t_c = 40s$. (Top plot) Signal represented in logarithmic scale shows the waveform as a shaded object. (Bottom plot) Last 5 milliseconds of the same signal. Clearly shows the sinusoidal oscillations before coalescing. [40].

complicated equations for two orbiting objects to simpler equations for a single spinning object [30].

Compact Binaries produce the most interesting GW signals. As the massive celestial bodies revolve around either other, they produce GWs in the form of sinusoidal oscillations popularly known as a *chirp signal*. The CBC GWs increase in both amplitude and frequency, resulting in an audio similar to birds chirping sound (hence the name chirp signal). Figure 2.2 shows a sample inspiral chirp. The Y-axis represents the strain of the signal and the X-axis represents time. In this particular simulated signal, the top signal lingers for over 40 seconds and hence appears as a shaded signal whereas the bottom signal lasts only milliseconds (revolving for only a few cycles before the masses absorb each other) and clearly showcases the sinusoidal oscillations.

Since the noise here is non-stationary and non-Gaussian, the isolation system estimates the characteristics of noise to remove it from the raw data. The clean data thus obtained is searched for a potential GW signal using optimal matched filtering techniques or the Bayesian method that relies on the likelihood principle

[10]. The event is classified as a detection event based on its likelihood of being a GW.

2.2 ChirpLab Statistics

Inspired by D.L. Donoho and X. Huos' paper 'Beamlets and Multiscale Image Analysis' [32], Candès developed ChirpLab software [24] for low-cost computing of chirp signals. This software is used for detecting rapid frequency changes on any type of chirp signals. It can be used for studying echolocation signals of animals, acoustic signals of all kinds, and any wave system with a significant change in frequency over time. The focus of the developers, however, was gravitational chirp signals. Usually, non-parametric detection methods assume the signal to be a slowly changing signal and hence the same approach will not work for GW chirp signals, which by definition are rapid changes in amplitude and frequency. ChirpLab makes use of Generalized Likelihood Ratio for finding the best fit for the waveform.

The section is divided into three parts. The first subsection introduces the fundamental blocks of the templates called *chirplets* and graphs constructed using chirplets. In the second subsection the Generalized Likelihood Ratio Test (GLRT) and hypothesis testing are discussed. The last subsection describes the Best Path statistics which uses GLRT to determine the presence of a signal. The statistical analysis and algorithm discussed in this chapter are mainly based on [14, 24, 25, 28].

2.2.1 Chirplet Graph

Most template-based detection methods are computationally expensive. Generally, template bank searches consist of the collection of waveforms (templates) generated by varying just one parameter at a time, and most models have multiple parameters. For gravitational waves, we have parameters like the mass of the two bodies, their distance, radiated energy, and sky localization. Each of these parameters has a considerable effect on the waveform. The number of possible waveforms increases exponentially as we increase the number

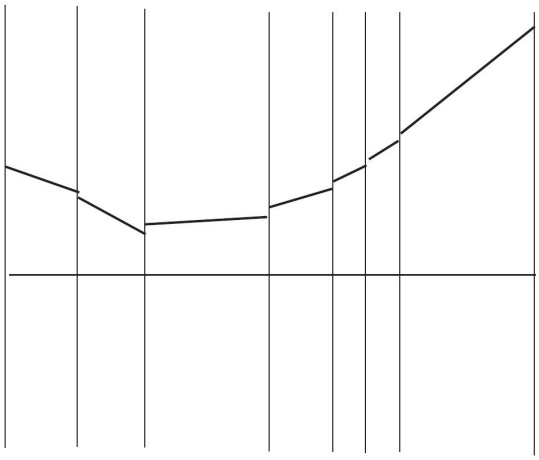

Figure 2.3: Illustration of a typical construction of graph using chirplets of variable length (as represented by the vertical lines) with the progression of time [25].

of parameters taken into consideration. In contrast, Chirplab is a generic detection technique and does not require full waveform (GR) templates. This is the fundamental reason for the computation being effective and fast. The algorithm uses P values to calculate the Best Path statistic and to judge if the data contains any target signal, as explained in Section 2.2.3. ChirpLab uses line segment type shapes called *chirplets* and constructs them into a graph as shown in Figure 2.3.

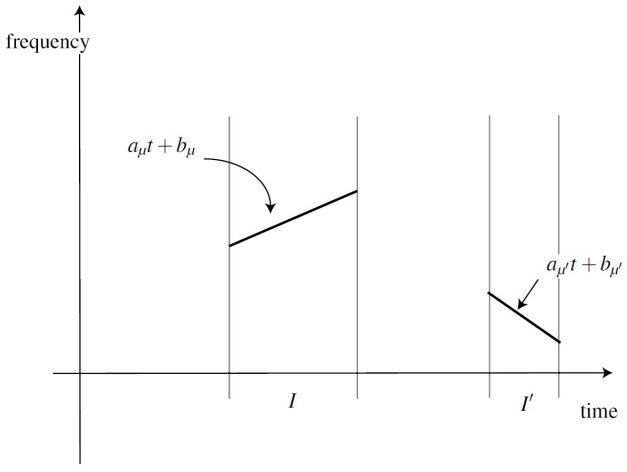

Figure 2.4: Pictorial representation of line segments known as chirplets in the time-frequency plane (X-axis represents time, Y-axis represents frequency). ChirpLab uses a dictionary type structure of chirplets that is based on length, slope and vertex position offset [25].

As seen in Figure 2.4, ChirpLab uses a dictionary of all the possible line segments. Here, $a_\mu t + b_\mu$ represents the chirplet parameters (a_μ being the slope parameter and b_μ the offset). The instantaneous frequency of a chirplet can be considered to vary linearly with time and be equal to $a_\mu t + b_\mu$, as the chirplet is presented in the time-frequency plane [25]. Figure 2.5 shows the progression of a chirplet chain. A following chirplet is naturally constrained to be adjacent (connected) in the time domain to the preceding chirplet. An additional constraint here is to have a small difference in slope and a small frequency offset between two adjacent chirplets. Thus in Figure 2.5, only the first subplot satisfies both constraints. Candes et al. [25]

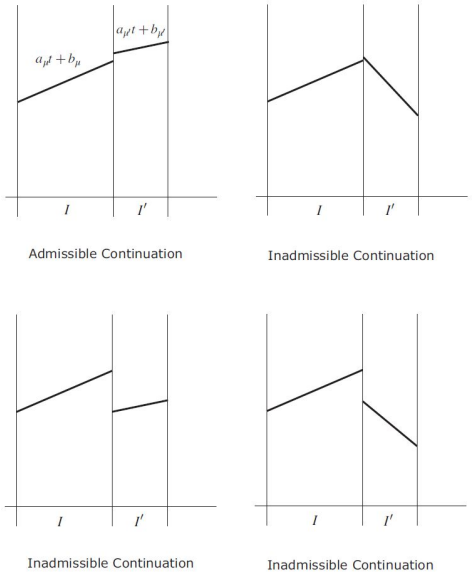

Figure 2.5: Validity of the successive chirplet in the chain of chirplets. Top Left: Valid continuation of the chain with minimal difference in slope **and** frequency offset at the juncture, Top Right: Unacceptable difference in slope, Bottom Left: Unacceptable vertex position offset and, Bottom Right: Unacceptable differences in slope and nonadjacent vertices [25].

explain the connectivity of chirplets as:

> We also consider a slightly different chirplet graph which assumes less regularity about the instantaneous frequency of the unknown chirp; namely, two chirplets are connected if and only if they live on adjacent time intervals and if the instantaneous frequencies at their juncture coincide [25].

The detection algorithm calculates the likelihood and Best Path statistics from thus formed chirplet paths/chains, as explained in Section 2.2.2 and Section 2.2.3.

2.2.2 Likelihood Ratio

Chassande-Mottin et al. [28] proposed a similar approach for detection based on chains of chirplets. However, their paper was aimed at detection of GW chirps with amplitude modulation and joint analysis of data from several antennas. They describe the likelihood statistic required for detection as:

> If the chirp phase and amplitude were known in advance, the detection would optimally be performed with the likelihood ratio. Under a Gaussian assumption for the noise, this likelihood ratio essentially reduces to the quadrature matched filtering statistic,
>
> $$l_p(x) = \left| \sum_{k=0}^{N-1} x(t_k) s_p(t_k) \right|^2 \tag{2.1}$$
>
> where we work with blocks of N data samples taken at discrete times $t_k = \frac{k}{f_s}$ with a sampling frequency $f_s \sim$ few kHz to cover the detector band. The above statistic amounts to correlating the data with the reference waveform $s_p(t)$ which is a copy of $s(t)$ normalized to unit norm. The result of the correlation is then compared to a threshold to decide whether the chirp is present or not in the data. In reality, the chirp phase and amplitude are not known. Inspired by the principles of the generalized likelihood ratio test (GLRT), we apply the statistic to all possible paths and check if at least one shows a significant correlation with the data [28].

The generalized likelihood ratio test (GLRT) effectively tests the "goodness of fit"[3] of the composite hypothesis with the null hypothesis. Here, the alternate hypothesis consists of a potentially large set of candidate chirplet paths. L takes on the ratio value of the likelihood with the mean vector λf by the null hypothesis

[3] the degree to which observed data matches the expected theoretical values.

as shown in (2.2). Here, λ is a scalar and f belongs to subset of unit vectors representing chirplets, F. For cases with $L < th$, those template fits are rejected; th is the threshold value here. In this setup, the GLRT takes the form,

$$L = \max_{\lambda \in R, f \in F} \frac{l(\lambda f; y)}{l(0; y)} \tag{2.2}$$

2.2.3 Best Path Statistics

The most significant statistic in ChirpLab is the Best Path (BP), as Candes et al. [25] conveniently name the statistic indicating the best possible chirplet path. The Best Path statistic measures if the input has any potential gravitational chirps. For all possible paths W, the best path is calculated using GLRT, where GLRT in (2.2) is equivalent to:

$$L = \max_{W} \sum_{v \in W} |\langle y, f_v \rangle|^2 \tag{2.3}$$

Here, y is the input signal and f_v is the element of a set of unit vectors for each chirplet index v. As explained in [25],

> In words, the GLRT simply finds the path in the chirplet graph which maximizes the sum of squares of the empirical coefficients. The major problem with this approach is that the GLRT will naively overfit the data. By choosing paths with shorter chirplets, one can find chirplets with increased correlations (one needs to match data on shorter intervals) and as a result, the sum of squares will increase. In the limit of tiny chirplets, $|\langle y, fv \rangle|^2 = \|yv\|^2$ and one has a perfect fit [25]!

Now for a path with fixed length of |W|, the value of the sum of squares will grow linearly with the length of the path. Hence, the test statistic is given as:

$$Z^* = \max_{W} \frac{\sum_{v \in W} |\langle y, fv \rangle|^2}{|W|} \tag{2.4}$$

The Best Path statistic is calculated in two steps, the first step is to calculate P-values for all candidate paths, and find the path with the minimum P-value. The second step is to compare the minimum P-value with the values in case of the null hypothesis [25].

P-value

In simple words, P-value is the probability of the alternative hypothesis being true against the null hypothesis. Depending on the threshold (usually taken as < 0.05), a P-value smaller than that rejects the null hypothesis meaning a rare event is reported.

Bonferrani method

This method enables us to compare multiple hypotheses. Here we compare the minimum P-value with different P-values under the null hypothesis, and reject the hypothesis as suitable.

Before calculating the BP statistics, the length of chirplets must be defined. There are two ways to do this. We can have chirps on a single scale where each of the segments/chirplets would be of equal length, 2^j. One complication of a single scale is having to decide the length of a chirplet (by deciding the value of j); it is possible to have chosen the wrong length of chirplets and the signal goes unnoticed. Another way is to have the chirplets be of variable length depending on the frequency behavior of the input data. This multiscale approach will be computationally more expensive as compared to the single scale, but it gives a much better fit as the chirplets of smaller size can match better for rapidly changing frequency. Candes et al. [25] claim that the computation is rapid even for BP statistics with multiscale chirplets. For a detailed algorithm, see [25].

To put it succinctly, BP shows the most suitable chirplet path, which in the presence of a signal indicates a

spike[4]. Depending on the number of chirplets and the division of total length into chirplets, the location of a spike (or potential signal) can be determined. There are other proposed methods for non-template based detection of gravitational chirp signals. Most approaches such as best chirplet chain (BCC) by Chassande-Mottin et al. [28] and time-frequency (TF) detection by Anderson and Balasubramanian [14] consider a single interferometer case mainly employing statistics for the search. Candes et al. [25] also developed shortest path (SP) statistic and minimum-time-to-cost ratio (MTTCR) as variations to BP for improved storage requirements and so on.

2.3 Summary of the chapter

Currently used methods involve generating templates by varying parameters like mass of the object, mass ratio, time of coalescence and so on. Thorne emphasized the ease of inferring parameters of a BBH system using Einstein's relativistic laws, yet there is no validity check on Einstein's laws. For this reason, we focus on a non-template based detection algorithm as expressed in the chapter. ChirpLab uses statistical analysis for non-template based detection. ChirpLab instead forms a graphical representation of a chirp signal by arrangement of the chirplets, the chirplet path or graph. These different paths are tested with GLRT based BP statistic to determine the graph that best describes the input signal. Intuitively, pattern based searches should require less computation power since they do not require bulky template banks as confirmed by Candes [24]. The BP detection algorithm forms the first block for independent (of GR) GW analysis pipeline. Next, we move on to parameterized evaluation of the analysis using ppE. Chapter 5, show the results of our simulated waveforms and BP analysis of the same.

[4]peak in the BP statistics due to steady increase in the frequency

Chapter 3

Parameterized Post-Einsteinian Testing

3.1 Introduction

Ever since the inception of the Theory of General Relativity (GR) in 1915, it has been under severe scrutiny. This hundred year old theory is now the accepted gravitational theory and is one of the most rigorously tested theories in physics; according to Asmodelle [16] it has never failed a single test. Einstein famously stated that if the measurements of light deflection disagreed with the theory he would "feel sorry for the dear Lord, for the theory is correct!".

Before we move to details it is important to define weak and strong gravity fields. The weak gravitational field regime is described with $\epsilon << 1$, where ϵ[1] is the strength of the field, for example, the gravity in the solar system is considered to be weak-field. The strong fields are when $\epsilon \to 1$. This generally occurs around massive celestial bodies or the expanding observable universe, for example, $\epsilon \sim 0.2$ on the surface of a neutron star [67].

Current approaches for verifying Einstein's theory ultimately use an approximation of that very theory for the analysis of data. Yunes and Pretorius [69], in 2009, argued that there is a fundamental bias introduced when

[1] $\epsilon \sim \frac{GM}{Rc^2}$

analyzing GW with GR (and PPN) derived waveforms. They proposed another approach, the parameterized post-Einsteinian framework, for the testing of GR with negligible assumptions. One of the reasoning (for testing) was based on the fact that Post-Newtonian approximations were developed for weak gravitational fields and do not guarantee effectiveness for strong, dynamic gravitational fields (such as BH/NS mergers).

The testing of the Theory of GR arose when Einstein compared Newton's concept of gravity to his own. These experiments were later named as classical tests of GR and will be briefly introduced here. Having established the BP detection techniques in the previous chapter, we now move towards another block in our parametric data analysis pipeline with the ppE testing. It is important to note that if a potential GW is detected, we will have to rely on conventional theory-dependent techniques for parameter estimation[2]. On the contrary, a generic approach may be developed that uses GR and non-GR templates for parameter estimation. At present, the ppE generated templates are not meant to serve the purpose of parameter estimation. The ppE formalism is instead aimed at measuring the deviation (from GR) in predicted parameters. As will be seen in the chapter, ppE unifies theories that follow certain criterion and is also able to interpolate (waveforms) between competing theories. Section 3.2.1 discusses the widely used Parameterized Post-Newtonian (PPN) framework followed by the alternate ppE framework in Section 3.2.2.

3.1.1 Classical tests

When Einstein published his theory he proposed three tests, later referred to as classical tests. These tests were to test theoretical predictions with measurements obtained from experiments. A simple comparison of General Relativity and Newton's theory had inspired these tests.

1. The perihelion advance of Mercury's orbit

   Even after considerable effort, Newton's theory of gravity could not account for the additional 43

[2]prediction of various parameters such as sky localization, final mass of the resulting black hole, final spin of the resulting black hole and so on using matched filtering.

seconds per century in perihelion[3] advance in Mercury's orbit. However, GR explained that the shift in Mercury's orbit was attributed to the curvature of spacetime by Sun (and Mercury). Einstein's predictions exactly matched the true value (obtained later through experiments). For more, see [41].

2. The deflection of light by the Sun

   Newton predicted that light will bend around heavy bodies. Einstein said the energy follows geodesics in curvature and the deflection should be considered with the light source as the reference frame. He correctly predicted the deflection of light coming from the sun to be 1".75[4] whereas Newton's theory gives the deflection of light to be 0".87 [16]. This was measured by Eddington during a solar eclipse in 1919.

3. The gravitational redshift of light

   Gravitational redshift, similar to cosmological redshift, is when a clock seems to tick slower (photon has longer/redder wavelength) to a distant observer. Einstein predicted that under the gravitational force of massive bodies, photons tend to gain or lose energy depending on the direction of motion [16]. This was tested by measuring the frequency of photons travelling in a tall tower of 74 feet. This was conducted in 1960 by Pound and Rebka at Jefferson Physical Laboratory [56].

3.2 Testing of Gravitational waves

Karl Popper speculated that a scientific theory can never be fully confirmed, but instead it can only be falsified. The falsification method suggests that to test any theory, it must undergo a "severe" test which it must pass [54, 55]. Mayo [48] proposes that severe testing be formulated in terms of whether the data X_0 provide sufficient evidence to support a hypothesis H_1 and to reject the null hypothesis H_0. Einstein's

[3] closest point of Mercury's orbit to the Sun

[4] Angle of deflection represented in seconds ("), 1/3600 of a degree.

theory is further strengthened with the release of the first ever image of a black hole. Along with the tests for GR, it is important to test the behavior of the resulting gravitational waves. As described in Section 3.2.1, the analysis of GWs is based on approximation theories and fundamental assumptions. Hence, it is important that we test this approach for its consistency with GR. Current methods involve using Post-Newtonian theory which is not meant for strong fields but instead is meant for weak field regimes, like the solar system, that are coherent with the formal assumptions of the theory. However, it is used for analysis of BBH systems, which have strong gravitational fields; it remains a mystery why the theory is effective in this case [66].

There would be a deviation[5] introduced in parameter estimation, when observed data is analyzed using template waveforms derived from Einstein's equations, if GR does not fully and accurately describe gravity near massive objects. This Section describes the testing framework for analysis; these theories generate waveforms that can be used as templates for matched filtering but shouldn't be. The main concern is computational cost and complexity, as both increase with the inclusion of these new non-GR waveforms. Hence, we stick to using PN theory based detection methods. This is acceptable, since the deviation caused by current methods will not cause a signal to go undetected; it will simply result in incorrect estimation of the parameters.

3.2.1 Parameterized Post-Newtonian Formalism

Post-Newtonian Theory

It is not always possible to find analytical solutions for Einstein's field equations (EFE), hence approximation methods are employed. Einstein was the first to use the approximation that came to be known later as Post-Newtonian (PN) expansion with the classical tests. However, it was first formally described by

[5]Theoretical bias (as per [69]) in analysis (estimated parameters and such) indicating a preference for GR with a probable non-GR wave.

Chandrasekhar and others [27]. The most important terminology of this theory is "Post-Newtonian order", usually referred to as "PN order", which constitutes the amount of deviation of the solution from Newton's laws of gravitation. As is usually the case in science, the higher the order the more accurate the approximation is. As described in "Post-Newtonian Theory and its Application"[20], the cost for employing this approximation method is the need to solve for a very high PN order. However, it must be noted that back in 2003, when Blanchet 20 wrote the paper, PN theory was the only existing solution and LIGO was still in its initial stages with significantly less sensitivity as compared to present day aLIGO.

The basic form of n th PN order is

$$nPN \sim \frac{1}{c^{2n}}$$

The expression demonstrates that PN order is reciprocal to the exponential power of c. For example, the equation for 2.5PN is as follows, where ω is the changing orbital frequency with time and O is used to describe the residual terms for that order. [20],

$$\frac{\dot{\omega}}{\omega^2} = \frac{O}{c^5}$$

The higher the PN order, given as $\frac{1}{c^{2n}} \to 0$, the more this expansion starts to resemble the Theory of General Relativity [15]. For 0 PN, the speed of gravity reaches infinity (as $c^0 = 1$, resulting in ungoverned value of c) basically reducing the PN expansion to approximate Newton's laws of universal gravity.

$$h^{\alpha\beta} = \sqrt{-g}g^{\alpha\beta} - \eta^{\alpha\beta} \tag{3.1}$$

PN expansions are more commonly expressed in terms of tensors in place of $O\left(\frac{1}{c^n}\right)$, where $g^{\alpha\beta}$ is the contravariant metric, g is the determinant of covariant metric and $\eta^{\alpha\beta}$ is the Minkowskian metric [**?**].

Parameterized Post-Newtonian framework

The Post-Newtonian theory uses metric tensors, as seen in (3.1) in the previous section, to find a solution for EFE. PPN unifies all the metric theories by introducing 10 free valued parameters. The only difference in all metric theories, i.e. theories that comply with the Einstein's equivalence principle[6] (EEP), is in the numeric value of coefficients of the metric potentials [62]. These extra parameters have their values set to identify each of these different theories. The limits for these parameters are found by different observations and experiments. The Cassini spacecraft tracking gave a limit for $\gamma - 1 \quad \text{as} \quad 2.3 \times 10^{-3}$. Table 3.1 lists the parameters with the constraints as per [62, 66].

Parameter	Significance	Limit
$\gamma - 1$	Amount of space curvature produced	2.3×10^{-3}
ξ	Preferred location (reference)	10^{-3}
$\beta - 1$	Amount of nonlinearity	3×10^{-3}
$(\alpha_1, \alpha_2, \alpha_3)$	Preferred frame (reference)	$(10^{-4}, 10^{-7}, 10^{-20})$
$(\zeta_1, \zeta_2, \zeta_3, \zeta_4)$	Conservation of momentum	$(10^{-2}, 10^{-5}, 10^{-8}, -)$

Table 3.1: PPN parameters with the established constraints [66]

.

Equations 3.2, 3.3, and 3.4 represent the PPN g_{ij} metrics with U, V_i, W_i, Φ and A as metric potentials. These equations are presented to give the reader a sense of how all the parameters tie in and refer to [62, 65, 67] for more details.

$$g_{00} = -1 + 2U - 2\beta U^2 - 2\xi\phi_W + (2\gamma + 2 + \alpha_3 + \zeta_1 - 2\xi)\Phi_1 + 2(3\gamma - 2\beta + 1 + \zeta_2 + \xi)\Phi_2 + 2(1 + \zeta_3)\Phi_3 + 2(3\gamma + 3\zeta_4 - 2\xi)\Phi_4 - (\zeta_1 - 2\xi)A - (\alpha_1 - \alpha_2 - \alpha_3)w^2 U - \alpha_2 w^i w^j U_{ij} + (2\alpha_3 - \alpha_1)w^i V_i + O((\frac{v}{c})^3)), \quad (3.2)$$

[6]The principle of Equivalence is summarized as "Whenever an observer detects the local presence of a force that acts on all objects in direct proportion to the inertial mass of each object, that observer is in an accelerated frame of reference [38]."

$$g_{0i} = 1/2(4\gamma + 3 + \alpha_1 - \alpha_2 + \zeta_1 - 2\xi)V_i - 1/2(1 + \alpha_2 - \zeta_1 + 2\xi)W_i - 1/2(\alpha_1 - 2\alpha_2)w^i U - \alpha_2 w^j U_{ij} + O((\frac{v}{c})^{(5/2)}) \quad (3.3)$$

$$g_{ij} = (1 + 2\gamma U)\delta_{ij} + O((\frac{v}{c})^2) \quad (3.4)$$

3.2.2 Parameterized Post-Einsteinian Formalism

The assumptions in PN theory are valid for weak fields but can cause various detection and estimation errors for strong fields such as BBH systems. As seen in Section 3.2.1, PPN unifies all metric theories by use of the 10 parameters shown in Table 3.1. This section will present the parameterized post-Einsteinian (ppE) framework formulated by Pretorius and Yunes. Pretorius and Yunes provide ppE parameters that interpolate between General Relativity and alternate theories [69]. The purpose of ppE theory is to obtain ppE parameters without *a priori* assumption that the theory of general relativity is correct. This will enable us to detect if GWs deviate from GR in a strong dynamic field. The ppE unification considers theories that fulfill (other than EEP) the weak-field consistency[7] and/or strong-field inconsistency[8]. To do so, Pretorius and Yunes modify pure GR equations with ppE parameters α, β, ϵ, a, b, c and d. Although the waveforms obtained from this approach may be used as a template bank for matched filtering, such an approach is not recommended. The non-GR waves, if they exist, will not go undetected by current methods but simply give incorrectly estimated parameters. Hence, the testing with ppE templates is more suitable post-analysis as it will validate if that signal follows pure GR or not.

[7] "theories that reduce to GR sufficiently when gravitational fields are weak and velocities are small, i.e. to pass all precision, experimental and observational tests [69]."

[8] "theories that modify GR in the dynamical strong-field by a sufficient amount to observably affect binary merger waveforms [69]."

The modified gravitational waveform, with ppE corrections, for the three stages (inspiral, merger, and ringdown) is given as follows:

$$h_I(f) = h_{gr}(f)(1 + \alpha u^a)e^{i\beta u^b} \tag{3.5}$$

$$h_M(f) = \gamma u^c e^{i(\delta + \epsilon u)} \tag{3.6}$$

$$h_R(f) = \zeta \frac{\tau_{damp}}{1 + 4\pi^2 \tau_{damp}^2 \kappa (f - f_R)^d} \tag{3.7}$$

This thesis focuses on the inspiral phase. In equation (3.5), $h_{gr}(f)$ is the waveform obtained from GR theory, the PN approximation for which has been derived and is given in (4.1) . The parameters $\gamma, \delta,$ and, ζ are defined with the continuity required from the inspiral and merger stages, respectively. ζ describes whether the simulation is consistent with conservation of momentum, as given by perturbation theory, for the ringdown phase [66]. Here, d is a ppE parameter and κ is the ppE function of remnant mass.

Theory	ppE α	ppE β	a	b
GR	0	0	-	-
Brans-Dicke	0	β_{BD}	-	-7/3
Mass gravity	0	β_{MG}	-	-1

Table 3.2: Values for ppE parameters

There are various theories to consider for the purpose of showcasing the unification of theories with ppE; such as Einstein-Æther [33, 34, 35], Tensor-Vector-Scalar (TeVeS) [17, 18, 58] and Chern-Simons modified gravity [13, 70], but for this project we will only consider General Relativity, Brans-Dicke (Section 4.4), and Massive gravity theory (Section 4.5). The rationale behind choosing these theories was to reduce the complexity by reducing the number of parameters. Since $\alpha = 0$ for all theories considered in this thesis, the values of parameter 'a' will be irrelevant as per (3.5). Table 3.2 displays parameters for the three theories. The β values are described in Sections 4.5 and 4.4. Values for a and b are taken from [69]. This thesis will hence be focusing on β parameter for all the theories.

3.3 Summary of the chapter

Overall, it may be said that ppE framework serves the purpose of a parametric testing structure unrestrained by assumptions as is intended in this thesis. A comparison of PPN and ppE shows that ppE employs the smallest set of parameters for unification of theories. Another distinction between the two testing framework is that PPN unifies only metric theories, whereas ppE additionally considers theories that satisfy the weak-field consistency and strong-field inconsistency [69]. After the detection using ChirpLab is performed as discussed in previous chapters, we proceed to check if the observed signal follows GR exactly through ppE. The thesis focuses on inspiral CBC waves for Brans-Dicke and Massive gravity theories since both the theories only require ppE parameter β. For the inspiral stage, ppE simply adds a correction term to the GR frequency response. Our methods compute the ppE modified equations with ChirpLab libraries as will be described in the following chapter.

Chapter 4

Computational methods

4.1 Introduction

The theoretical approaches discussed in previous chapters are adopted by our computation method. In this thesis, we propose to use ChirpLab libraries for developing ppE type post-processing of the inspiral event.

The ppE framework intends to unify all major competing theories, in fact, the framework interpolates between these theories. We will examine two of those theories, namely Brans-Dicke and Massive gravity. Both the theories have ppE parameter $\alpha = 0$, thus reducing the number of parameters to compute.

We begin with examining two of the currently used analysis softwares: PyCBC and LIGO algorithm library (the software package here on referred to as `lalsuite`). For parameterized testing, `lalsuite` uses PPN based routine which will be described in Section 4.2. Our methods take inspiration from the phenomenological model used currently (IMRPhenomD and TarylorT3, described in Section 4.2.2) and alter the software to simulate the ppE waveform. Another popular software used for compact binaries' analysis is Python-based PyCBC. PyCBC wraps the C libraries of `lalsuite` with Python routines such as simulation of GWs, filtering and so on. Finally, we discuss the extended ChirpLab method with a brief review of the chosen theories (Brans-Dicke and Massive gravity). The discussion mainly focuses on the ppE parameter β, subsequently showing the affect of β on the waveform in the next chapter.

4.2 Current methods

There are various computational methods for the purpose of simulation of GWs, detection, matched filtering, waveform analysis, parameter estimation and so on. However, for the purpose of parameterized testing of GR through computation, there exists only the PPN theory based approximant[1] (in `lalsuite`) called 'GeneratePPNInspiral'. The 'GeneratePPNInspiral' routine was developed by T. D. Creighton and it follows the orbital frequency $f(t)$ and PN coefficient equations from [60]. Therefore, we aim to introduce a testing approximant 'GeneratePPE' as a step of this research project. In 2015, Berti et al. [19], Li [45] proposed a Bayesian method for testing GR called Test Infrastructure for GEneral Relativity (TIGER). Software like TIGER and our methods should be able to test the reliability on currently used GR templates.

4.2.1 PyCBC

PyCBC is a python based open software used for gravitational wave astronomy [9, 63]. PyCBC offers a variety of pipelines and features for analysis of GW data. PyCBC is used in the project described in this thesis for template bank generation and matched filtering.

Template bank generation for PyCBC uses the PN approximation for total mass with $m_{tot} \lesssim 4\ M_\odot$ [2] and uses Numerical Relativity (NR) calibrated EOB for greater m_{tot}. We have used PyCBC for simple generation of simulated GW with masses $m_1, m_2 = 1.4 M_\odot$ and no spins, as shown in Figure 5.1, for the purpose of comparison with our simulated signal. Time domain approximants TaylorT3 [39] and IMRPhenom model (IMRPhenomD) [37, 42] are shown in the result Section 5.2.1.

[1] An approximation method employed based on different theories and their variations with alignment and spins. For example, TaylorT1, SpinTaylorT1, EOBNR, SEOBNR and so on.

[2] $M_\odot$ represents unit solar mass

4.2.2 LALsuite: IMRPhenomD

Phenomenological models which describe the inspiral, merger, and ringdown phases are used for computing waveforms and do not rely on the physical dynamics of the BBH system. These models (IMRPhenom) are constructed as a hybrid waveform between PN theory and Numerical relativity, see [11]. IMRPhenomD[3] is a frequency-based computational model of aligned spin binary systems and primarily consists of files written in 'C' (`lalsuite:LALSimulation`). IMRPhenomD uses Post Newtonian and NR for mass ratios up to 1:18. This model divides the phenomenon into three stages; inspiral, intermediate, and merger-ringdown. The intermediate stage is an interpolation between inspiral and Merger stages since it is an open debate as to where exactly the merger starts. The merger-ringdown is modeled purely from NR data simulations and uses the approach as described by Khan et al. [42]. This provides another reason (other than the continuity required among the parameters and dynamics in perturbation theory) for this thesis to concentrate on inspiral only, as the ppE framework is divided into inspiral, merger, and ringdown. The merger and ringdown are described separately in the ppE framework besides ppE does not consist of an intermediate stage. Hence, transforming the ppE equations to be in agreement with the stages of IMRPhenomD will be beyond the scope of this text.

4.3 ChirpLab with ppE

We modify the inspiral equation (3.5) using the ChirpLab file *inspiral*. The MATLAB program takes three theories as input parameter,'GR' 'BD' and 'MG'[4], depending on which parameter values to consider. Ideally, when creating a ppE template, these parameters (in this case, α and β) vary values as per well-known theories after constraints obtained through observation. These values take into account competing theories,

[3]There are five models, IMRPhenomA models non-spinning binaries [11]; IMRPhenomB is a dated model for non-precessing binaries [12]; IMRPhenomC improves upon the previous model [59]; IMRPhenomD is the most recent and accurate model for non-precessing binaries [42]; IMRPhenomP models precessing binaries [43].

[4]GR represents General relativity; BD represents Brans-Dicke; MG represents Massive gravity

even theories that are yet undiscovered, giving us a more general and freely parameterized approximation. This same approach can be taken to improve `lalsuite` to include ppE framework as a new subroutine for post processing of GW. Due to the complicated program hierarchy, it seems unsafe to create and include ppE routine in the base `lalsuite` package. Yunes and Pretorius [69] gave the corrections for frequency response, $\tilde{h}(f)$, as shown in (3.5). However, we would like the reader to note that this thesis assumes ppE corrections to be the same for time domain response $h(t)$. The aim of this thesis is to provide proof of concept for ppE and showcase the practical potential for the same. The ppE waveforms (templates) when used with matched filtering on detected potential signals, can be tested for the signal's deviation from General Relativity.

All the simulations are done using the following,

$$M_{\odot} = 1.98 \times 10^{30} kg \quad \text{(Mass of Sun)}$$

$$m_{tot} = m1 + m2 \quad \text{(Total mass of binary)}$$

$$\text{where,} \quad m1, m2 = 1.4 M_{\odot} \quad \text{(Individual masses)}$$

$$\eta = \frac{m1 \times m2}{m_{tot}^2} \quad \text{(Symmetric mass ratio)}$$

$$M_{chirp} = \eta^{3/5} \times m_{tot} \quad \text{(Chirp mass/Radiated mass)}$$

There are two ways to obtain the response function $h(t)$, using Amplitude A, and phase ϕ, for the plus and cross polarization as shown in (4.1) or with velocity squared v^2, and phase ϕ in (4.2). These equations follow from PN theory adapted from [50]. Constituent equations for A_+, $A_\times$, ϕ, and $t(v)$ are given in Appendix A.

$$h_{gr}(t) = A_+ cos(2\phi(t)) + A_\times sin(2\phi(t)) \tag{4.1}$$

$$h_{gr}(t) = v^2(t) cos(2\phi(t)) \tag{4.2}$$

The frequency function as described by Li [45], Teviet Creighton and Bruce Allen [60] and employed in [42]

is given by,

$$f(t) = \frac{M_\odot}{16\pi T_o m_{tot}}\Bigg(\Theta^{-3/8} + (\frac{743}{2688} + \frac{11}{32}\eta\frac{3\pi}{10})\Theta^{-5/8} + \\ (\frac{1855099}{14450688} + \frac{56975}{258048}\eta + \frac{371}{2048}\eta^2)\Theta^{-3/4} + (\frac{7729}{21504} + \frac{13}{256}\eta\pi)\Theta^{-7/8}\Bigg) \quad (4.3)$$

where Θ represents,

$$\begin{aligned}\Theta &= \frac{\eta M_\odot}{5T_\odot m_{tot}}(t_c - t) \\ &= \frac{\eta M_\odot}{5T_\odot m_{tot}}(t_c - t)\end{aligned} \quad (4.4)$$

The $h_{gr}(t)$ obtained from (4.2) represents the GR waveform. We reiterate the equation provided in Section 3.2.2 and show the modified $h_{gr}(t)$ as:

$$h_{ppE}(t) = h_{gr}(t)(1 + \alpha u^a)e^{i\beta u^b} \quad (4.5)$$

The following sections describe the β parameter that will be used in our extended ChirpLab computation.

4.4 Brans-Dicke

Brans-Dicke, a scalar-tensor theory, is one of the main competitors of Einstein's GR theory. The theory was developed by Carl Brans and Robert Dicke in 1961 and is the only other theory (than GR) that complies with the observations so far. This theory considers interaction of the scalar gravitational field with the tensor field from GR. Differently to GR, this theory consists of a scalar field known as ϕ that depends on the location. This in effect changes the gravitational constant (generally G). For our computation, we need to compute the ppE parameter β (to compute (4.5)) with the values approximating Brans-Dicke theory. Equation (4.6) shows how β_{BD} changes with the Brans-Dicke parameter ω_{BD}. Here, ω_{BD} is a dimensionless

coupling constant and S is the sensitivity based on binding energy. As $\omega_{BD} \to \infty$, the theory resembles GR [68]. These parameters are varied as per Table 4.1 for this thesis project. Equation (4.6) follows from [69]. Refer to [22] for more information about the theory.

$$\beta_{BD} = \frac{5}{3584}\frac{S^2}{\omega_{BD}}\eta^{2/5} \tag{4.6}$$

4.5 Massive gravity

Massive gravity theory considers a non-zero graviton mass, which as a result implies that gravitational waves obtained travel at a speed less than the speed of light. This theory has some drawbacks (violets strong field equivalence principle for one), but is still studied as scientists believe it can help constrain the quantum gravitational effect [69]. As expressed for Brans-Dicke theory, we calculate the value for ppE parameter β (to compute (4.5)) for Massive gravity. Equation (4.7) shows β_{MG} as a function of λ_{MG}. Here, λ_{MG} is the Compton wavelength[5] and D is the dipole moment.

$$\beta_{MG} = \frac{\pi^2 D M_{chirp}}{\lambda_g^2(1+z)} \tag{4.7}$$

Parameter	Constrained value	Unconstrained value
ω_{BD}	9×10^4	9×10^{-10}
λ_{MG}	15×10^{12}	15×10^{-3}

Table 4.1: Values used for the calculation of β (constituting parameters)

Finally, as will be seen from the results, as β approaches zero for both theories, it is very difficult to notice the difference between waveforms. Therefore, we used unrealistic values for ω_{BD} and λ_{MG} simply to demonstrate the difference in simulated waveforms (shown in Table 4.1). The results can be seen in Chapter 5.

[5]Normal wavelength of a photon considering its energy to be the same as the mass of that particle.

4.6 Summary of the chapter

As noted in this chapter, the only parameterized testing currently used is a PPN routine. There is a need to validate the observations with an approach free of theoretical dependence. We begin with a brief discussion of presently used (by LIGO) simulation and analysis software. The GR waveforms generated in LIGO methods and our extended ChirpLab follow the same formulae. Our method, then, incorporates the ppE correction term as described by Yunes and Pretorius to simulate non-GR waveforms. The motivation behind this chapter was to implement ppE using ChirpLab fixating on two theories, namely Brans-Dicke and Massive Gravity. For the above-mentioned theories, we compute the β parameter and consequently the ppE waveform. Please note we use unconstrained values (Table 4.1) for demonstration purpose only. In the next chapter, using the current simulation software such as PyCBC for calibration, we present results from our ppE extension of ChirpLab.

Chapter 5

Results

5.1 Preliminary discussion

Our methods discussed in previous chapters support the advances in developing parameterized testing of GR motivated by the questionable methods that use only GR for analysis. Moreover, we also further the approach by incorporating a non-template based detection algorithm offered by ChirpLab. The preliminary results discussed advocate the need for a processing pipeline of gravitational wave astronomy free of theoretical assumptions.

We demonstrate the inspiral waveform as generated by ChirpLab alongside PyCBC generated waveforms as a means for calibration. After a successful simulation of the GR waveform, we move towards working with non-GR simulations. As mentioned in the previous chapter, we enforce constraints (based on observation data) on the β parameter. To enhance the apparent difference between waveforms of different theories, we also use unrealistic values of the β parameter.

Finally, we use the detection statistics of ChirpLab for our simulated ppE waveforms. Ideally, for (post-analysis) testing with the ppE framework we would need to generate the ppE template bank. The ppE template bank can be used with correlation techniques or matched filtering to test the consistency of GW with GR. These templates can help in estimating parameters from the GW such as sky localization, final mass, final spin, luminosity and so on. According to Yunes and Pretorius [69], when testing ppE signals with GR templates, ppE can help in identifying the deviations in these above mentioned parameters. However,

this thesis demonstrates the generation of GW based on competing theories using only the ppE framework. We have used the waveforms generated using ppE to exhibit the robustness of the BP statistic with ChirpLab. The generic detection using BP should be able to pick out any chirp signals (GR or non-GR). Lastly, we conduct a search on real aLIGO data segments. It might interest the reader to note that the of our searches may have a potential GW (see Section 5.4).

5.2 Signal generation

First, simulated signals are presented to help readers visualize CBC signals. As the coalescence of a black hole pair progresses, the waveform has rapid change in frequency and increase of amplitude to create the shape of a chirp signal. The amplitude and frequency of GW attain the peak at the time of coalescence. In Section 5.2.1, we present three simulated signals. The strain[1] data is plotted against time for each signal. The waveforms can be described entirely with just the mass (of each black hole) m and the time of coalescence t_c.

We present non-GR waveforms as generated by extended ChirpLab next in Section 5.2.2. As seen in (3.5), ppE inspiral has two parameters, α and β. The theories considered in our computation converge to GR with $\alpha = 0$, hence we will concentrate on β. Essentially, both (α and β) parameters can be varied to construct waveform without establishing any particular theory. We have chosen Brans-Dicke (BD) and Massive gravity (MG) theories. The ppE correction term for both these theories can be represented only using ppE parameter β. We have taken the liberty of using unrealistic values of ω_{BD} and λ_{MG} (Table 4.1) for the purpose of amplifying the apparent differences in the corresponding waveforms. The generated waveforms are superimposed with 'Normal' (waveform generated using original ChirpLab) and 'GR' (waveform generated using ppE parameters converging to GR) to display the resemblances.

[1] a common terminology in GW physics representing the dimensionless amplitude 'strain', which is equal to twice of the observed displacement in the laser beam of the interferometer.

5.2.1 Inspiral: General Relativity

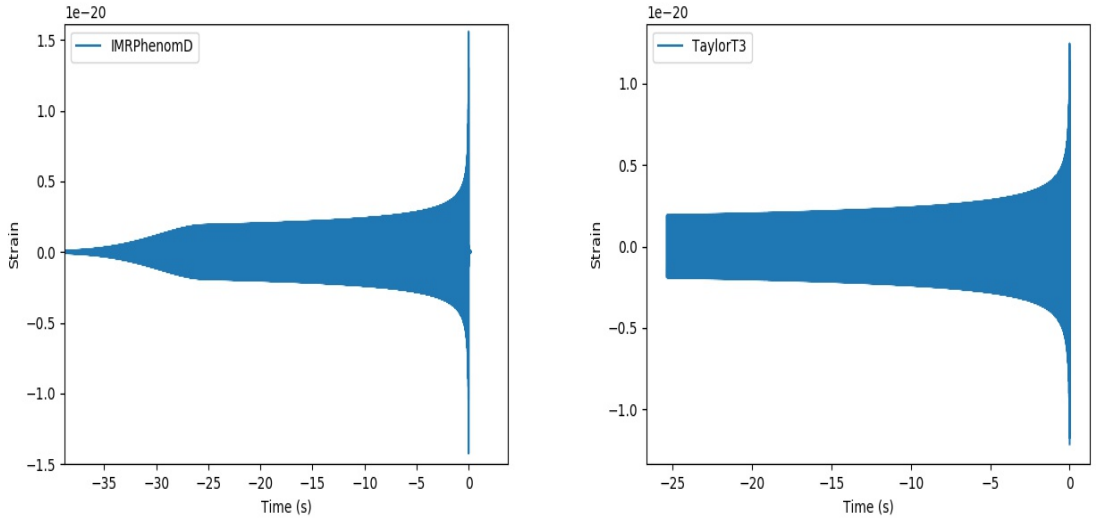

(a) (b)

Figure 5.1: Signals generated using PyCBC a) GR chirp signal generated using PyCBC with IMRPhenomD, see [42]. b) GR chirp signal generated using PyCBC with TaylorT3 (Hulse-Taylor Binary, see [39]).

We present the simulated waveforms from currently used software PyCBC as a pictorial representation of a CBC GW signal. We used two different software packages to generate the inspiral signal for the purpose of validating our computation (as shown in Figures 5.1 and 5.2a). PyCBC and Chirplab, both follow the same equations and give the same signal. PyCBC, as mentioned in 4.2.1, is a python package for LIGO collaboration that includes template bank generation, matched filtering, and so on. Figure 5.1 shows two signals generated using PyCBC software with two different approximants (IMRPhenomD and TaylorT3). PyCBC showcases the inspiral waveform to occur in negative time series with the merger at $t_c = 0$. In Figure 5.1a, IMRPhenomD starts the simulation from rotating binary pair, before inspiral has even begun, hence the signal slowly gains the amplitude before the start of inspiral at $t_c = -25s$, whereas TaylorT3 signal starts abruptly at $t_c = -25s$ in Figure 5.1b. The ChirpLab signal is expected to replicate the Taylor series waveform as it follows PN theory and does not use the NR formalism, whereas the phenomenological

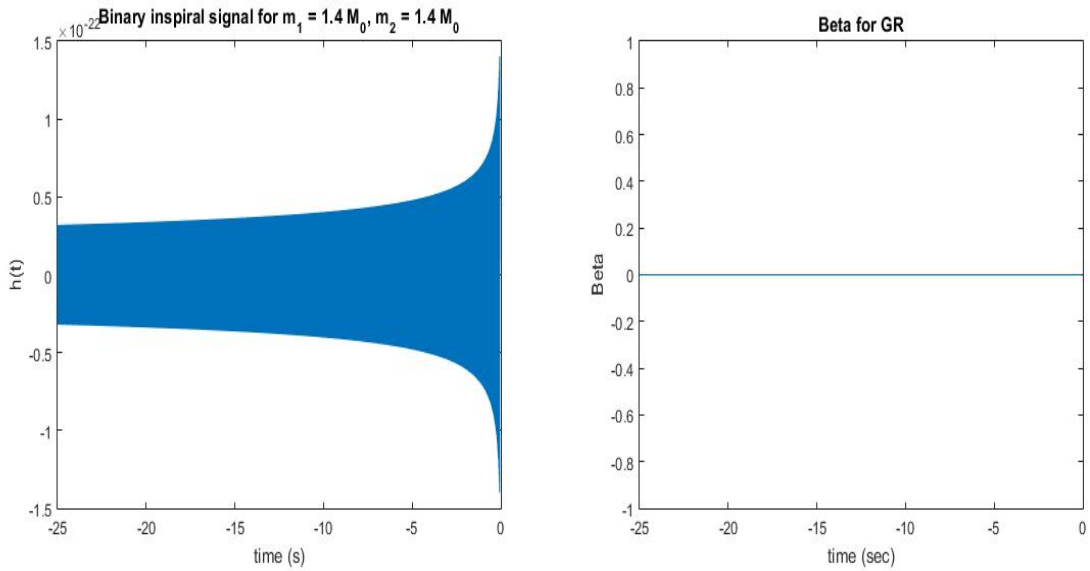

(a) (b)

Figure 5.2: ppE waveform generated using ChirpLab. The signal approaches GR waveform with parameters $(\alpha, \beta, a, b) = (0, 0, a, b)$. a) GR chirp signal b) Beta value

model IMRPhenomD is a hybrid of PN and NR. The ppE waveform replicates the GR simulation with $(\alpha, \beta, a, b) = (0, 0, a, b)$ as shown in Figure 5.2a. Ideally, we would superimpose the waveforms to check the convergence. However, superimposing the simulations is not possible here as we are using two different platforms for PyCBC and ChirpLab (Python and MATLAB respectively). Nonetheless, we will see ppE waveform converging to GR with unadulterated ChirpLab GR waveform in Section 5.2.2. Since our ChirpLab extension uses the ppE parameters α and β, we also present the β value in Figure 5.2b which remains zero as expected.

5.2.2 Inspiral: Alternate theories

We explore the parameter space to obtain different waveforms. For the simplicity of implementation, we have chosen alternate theories with $\alpha = 0$, the value of β varies as per theory as shown in (4.6), (4.7), and Table 4.1. Figure 5.3 shows the β profile for non-GR theories, BD and MG. Here, we have used constrained

values as per [69].

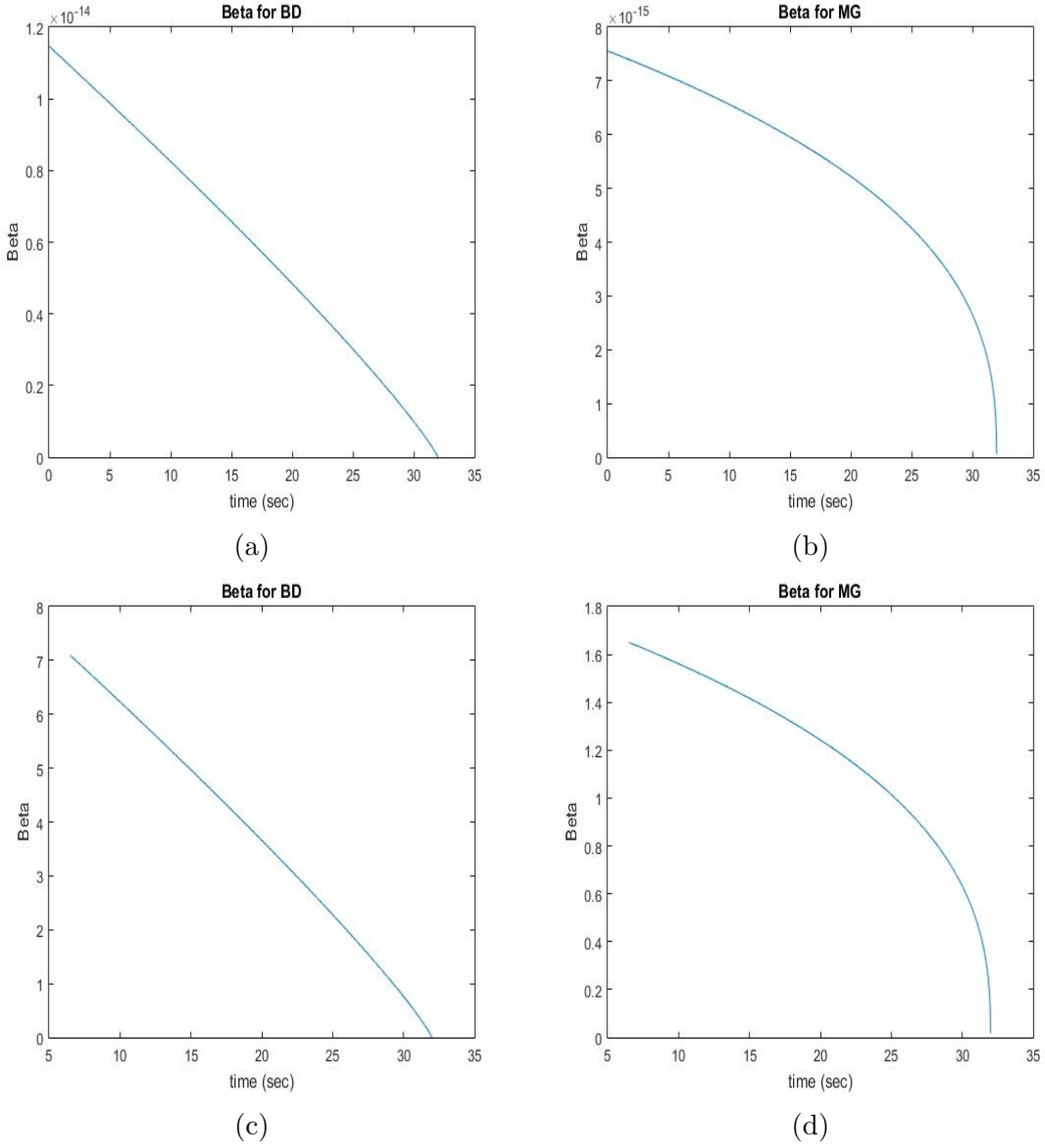

Figure 5.3: Beta shown for Brans-Dicke and Massive gravity theories, a),b) shows the constrained value of β as per [69] c), d) shows unconstrained for visualization as per Table 4.1.

As seen in Figures 5.3a and 5.3b, the value of β parameter decreases with time and finally becomes 0 at the time of coalescence (32 s). In both the figures, the value of β is the order of 10^{-15}, which visually shows no difference between BD and MG simulations when compared to the GR waveform. Therefore, we have also

included unconstrained values for β (Table 4.1) to amplify the apparent effect in waveforms (Figures 5.3c and 5.3d). Corresponding waveforms are shown in Figure 5.4.

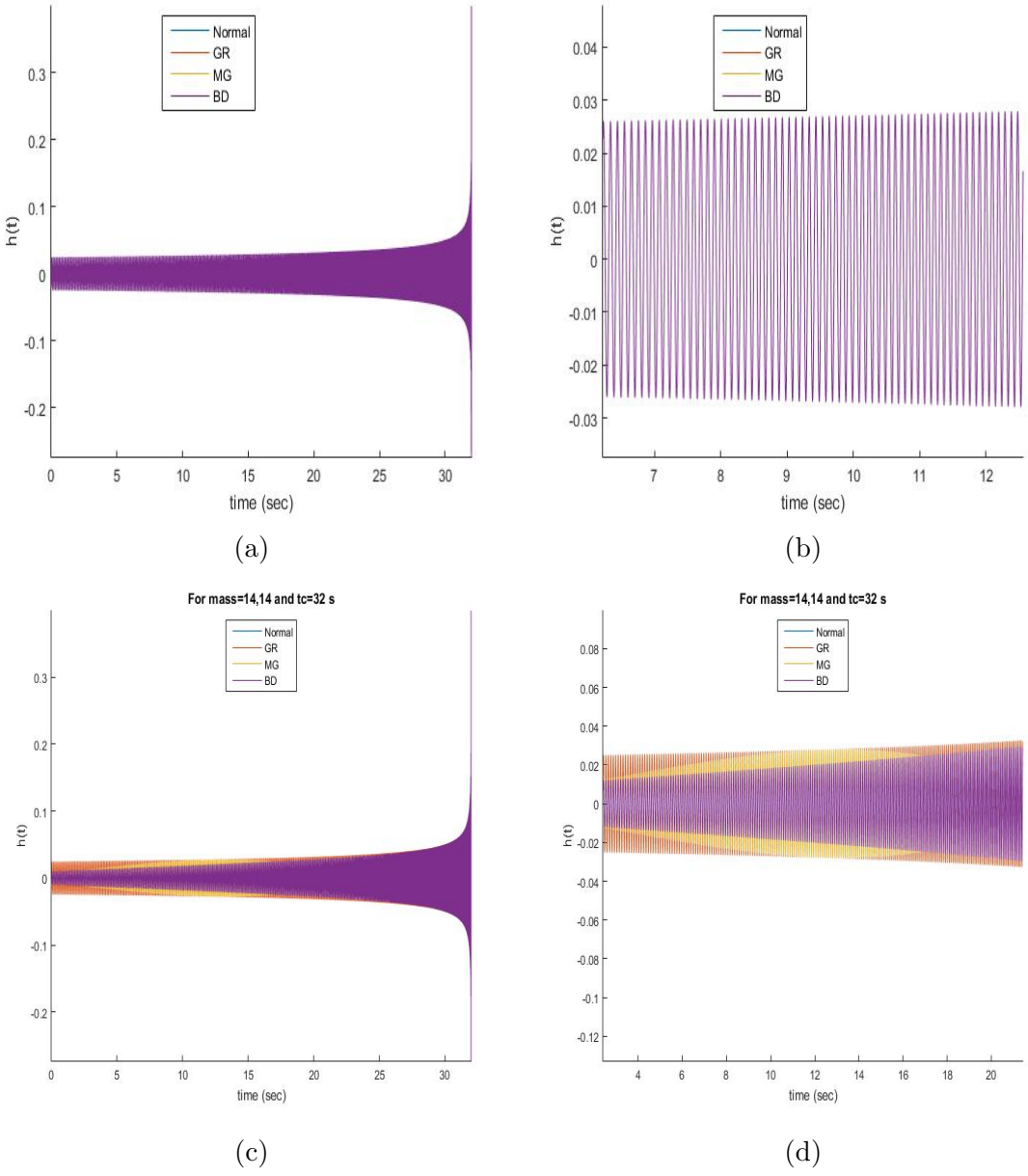

Figure 5.4: Waveforms are shown for Normal (PN), GR(PPE), Brans-Dicke(PPE) and Massive gravity (PPE) theories. a) Waveforms generated using constrained values of β b) Zoomed plot for constrained waveforms c) Waveforms simulated using unconstrained values of β d) Zoomed plot for unconstrained waveform.

Figure 5.4 shows all four waveforms superimposed on each other. 'Normal' is the waveform generated using the original ChirpLab method (using PN expansion). 'GR' is the waveform generated using our ChirpLab implementation of ppE with the parameters converging to GR theory. These two waveforms are identical as is expected. 'BD' and 'MG' have β as described in (4.6) and (4.7). All four waveforms give the impression of being identical in Figures 5.4a and 5.4b where β is truly constrained. Figures 5.4c and 5.4d show the waveforms being distinctly different with unconstrained values of β.

Even though all 4 waveforms appear to be identical with constrained value of β in Figure 5.4a, we probe further to see the difference. Figure 5.5 shows part of 5.4a super zoomed in to see the difference between waveforms. Normal and GR coincide, as they should, since both waveforms represent the same theory. MG and BD waveforms are also overlapping, at least appear to be, but this is caused by both the β ($\beta_{MG} \quad and \quad \beta_{BD}$) being very small, close to 0; and nearly of the same order of amplitude, 10^{-15}.

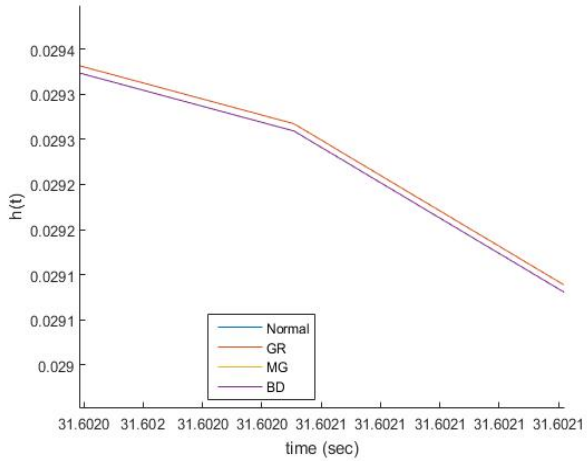

Figure 5.5: Zoomed in 5.4 part c)

Finally, the Fourier transform of $h(t)$ is performed, especially since the ppE correction was intended for $\tilde{h}(f)$ (shown in Figure 5.6). For unconstrained values for βs, the plot clearly shows all three 'GR', 'BD' and

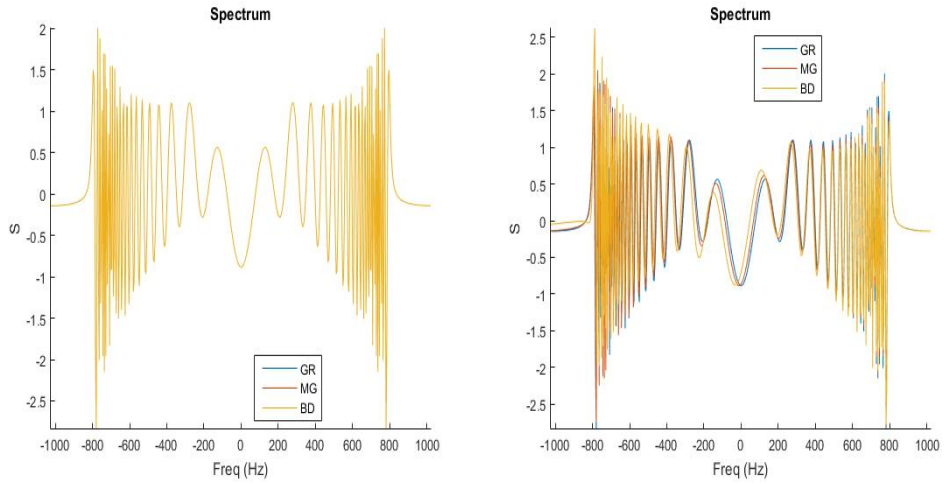

(a) (b)

Figure 5.6: Frequency response of ppE generated waveforms 'GR', 'BD' and 'MG'. Freq Spectrum with a) constrained β b) unconstrained β.

'MG' as different. This is a better view to judge the difference between 'BD' and 'MG', which was not very apparent with the time domain waveforms.

5.3 Detection of GW using ChirpLab

We, next, showcase the results from ChirpLab's detection algorithm using BP statistics. The first section 5.3.1 simply to demonstrate how the BP statistic behaves in the presence of a GR GW. The thick red line represents the BP (according to (2.4)) and the vertical dashes represent the division of chirplets. Generally, the chirplets are divided such that shorter chirplets are bunched where the frequency changes rapidly. The *spike* in BP plots are quite visible, with the peaks perfectly following the instantaneous frequency of the signal. However, the statistic may overfit the data for shorter chirplets. We test the same approach (BP statistics) on our non-GR waveforms, the results are shown in Section 5.3.2. Statistical algorithms like ChirpLab do not require template waveforms for detection. This helps reduce the requirements for computational power and storage.

5.3.1 Best path: GR

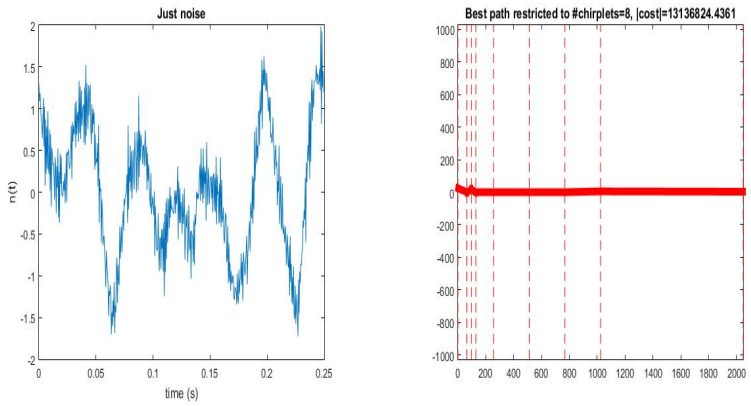

(a) (b)

Figure 5.7: a) Noise generated from PSD b) Best path with no signal present with number of chirplets=8.

The Best Path statistics were calculated for simulated gravitational waves with masses m1=1.4, m2=1.4 and time of coalescing $t_c = 0.25s$. First, we see how BP plot when only noise is present, Figure 5.7. Gaussian noise has been generated using the power spectral density and is shown in Figure 5.7a. The subplot 5.7b shows BP in case of H_0[2],i. e. no signal is present. In Figure 5.8a, the first subplot shows the simulated GW. The second subplot shows the instantaneous frequency. From BP plots in case of alternative hypothesis H_1, Figure 5.8, we can see how the BP peaks at the coalescence and indicates a chirp signal being present.

When a signal is present, the calculated Best Path (red thick line) spikes very significantly as seen in Figure 5.8. Figure 5.8 shows a simulated GR waveform, this signal is added to noise with SNR = 20dB. Subfigure 5.8b shows four BP searches with number of chirplets 1,2,4 and 8 respectively. Here, the best path is computed for four different dyadic chirplet graphs, the topmost plot in Figure 5.8b represents a graph consisting of only one chirplet. The second subplot shows the graph being divided into two parts (one for each chirplet) by the vertical dashes (at x=50). Usually, the accuracy increases with an increase in the number of discrete chirplets used. For example, 8 chirplets give a better approximation (as compared to 1,2,

[2]Null hypothesis

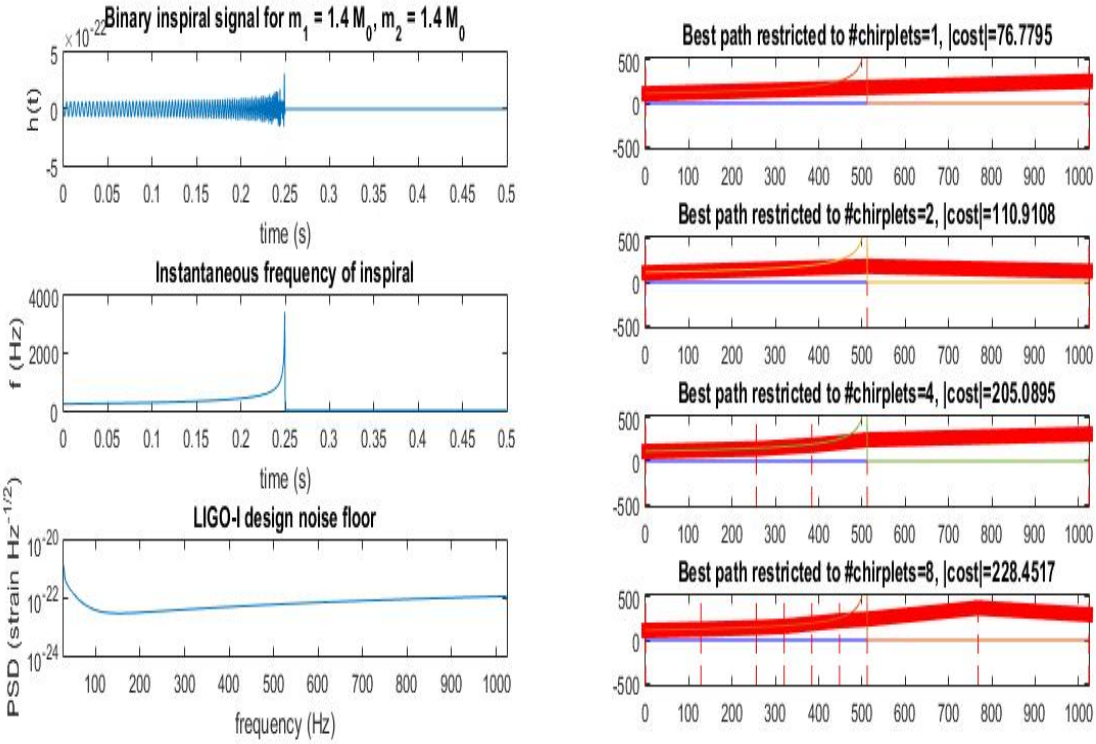

(a) (b)

Figure 5.8: Best path statistic (red thick line) for GR waveform. a) i) Inspiral signal generated using GR with masses=1.4, 1.4 and coalescing at $t_c = 0.25s$ ii) Instantaneous frequency shows the peak at the coalescence iii) PSD for noise with respect to frequency. b) Best path statistic for four subplots with number of chirplets=1,2,4, and 8 respectively. X-axis represents time in number of samples (s*Fs), Y-axis represents the Frequency (Hz).

or 4 chirplets) of what the input consists of and improves the statistics of the alternative hypothesis (i.e., presence of a GW). However, this is not always true (16 chirplets may give a better result as compared to 64 chirplets) and there is an increase in computational cost for a larger number of chirplets used.

5.3.2 Best path: ppE

The waveforms generated using ppE were run through ChirpLab to test the effectiveness of the chirplet algorithm for the non-GR waveform. This section shows the results regarding the same using the Brans-

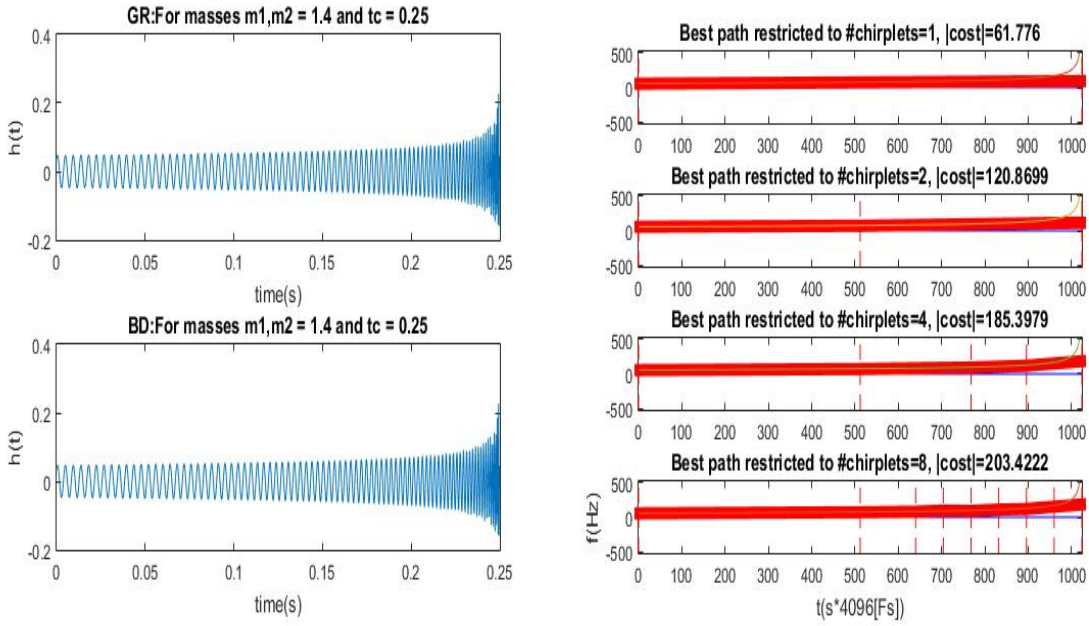

(a) (b)

Figure 5.9: ppE waveform approaches BD waveform with parameters as listed in Table 4.1. a) BD chirp signal generated using ppE. b) Best path statistic for chirplets length=1,2,4,8.

Dicke (BD) and Massive gravity (MG) waveforms.

Figures 5.9 and 5.10 show that ChirpLab's Best Path statistic is able to judge whether a signal is a gravitational wave even for non-GR theories. In Figure 5.9, the left plot shows the generated Brans-Dicke signal with a GR waveform for comparison. Both (BD and GR) signals are mixed with the noise for SNR=20 dB. The Best Path obtained is shown by the thick red lines, which clearly spikes up indicating the presence of a gravitational wave. The vertical dashes represent chirplet lengths, which also point to rapidly changing frequency with chirplets spread out at the end of the plot.

A similar plot is shown for Massive gravity theories simulated waveforms in Figure 5.10. Again the MG signal is shown in the left plot with GR waveform. This waveform does look similar as compared to Figure 5.9a. The Best Path statistic peaks in this case too, as expected the peak in BP does occur at the same place as the chirplet cluster (indicated by the vertical dashes).

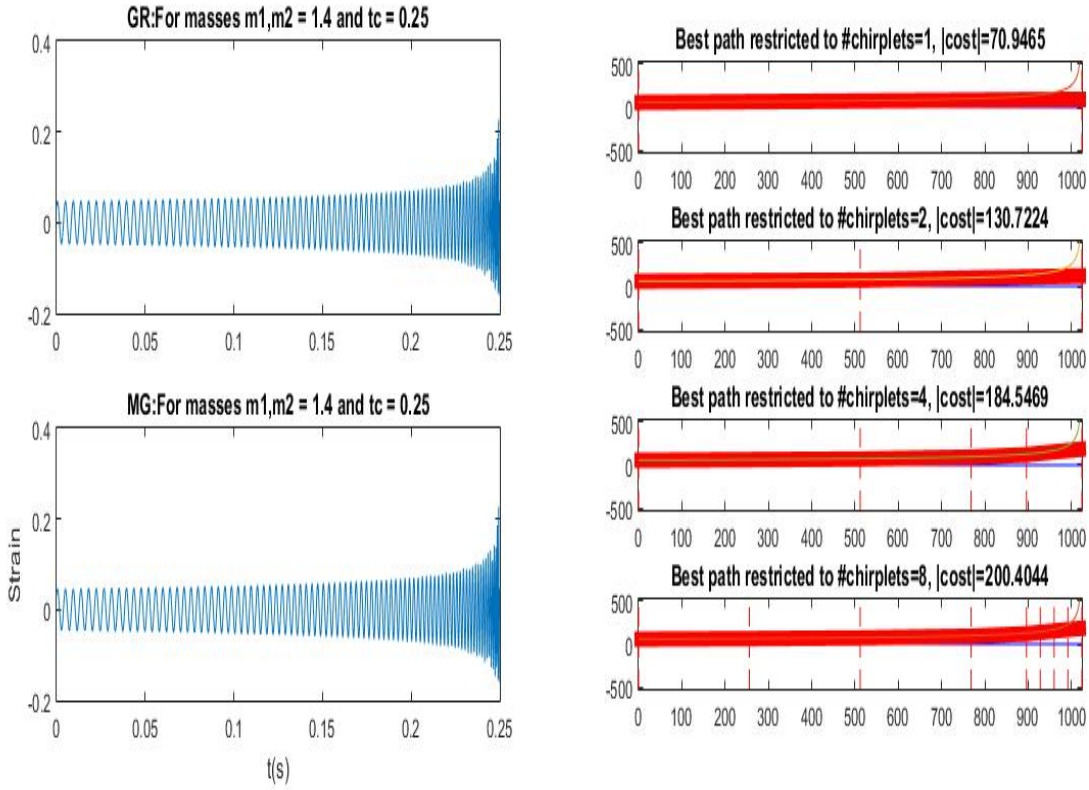

(a) (b)

Figure 5.10: ppE waveform approaches MG waveform with parameters as listed in Table 4.1. a) MG chirp signal generated using ppE. b) Best path statistic for chirplets length=1,2,4,8.

5.4 Non-template based search on Real data

Finally, we conduct a search on real aLIGO data. We first test a confident detection (GWTC-1 catalogue [29]) GW170809 and showcase the BP results (Figure 5.11c). The BP plot shows a *spike* at GPS 1181186302519.8, which is the coalescence time as per LIGO's analysis as well. Most of our results on randomly selected LIGO data files (with GPS 1126088704 and 1128669184) have no positive outcomes and have flat BP plots (example plot shown in Figure 5.11b). Interestingly though, one of the search results in a tiny *spike* as seen in Figure 5.11a, however we will need to further investigate the data segment before making any claims.

We utilized the 'Cascades' cluster with 1 large memory node consisting of 72 CPUs for each run; one

data-file[3] required $\sim$ 197 hours for computation. Each file was divided into 256 data segments, $length = 2^{16}$ $samples/segment$, to accommodate the memory limits per node/user. The plots in this section have been selected from all the results obtained. The search was conducted on three different data-files, GW170814 and two files with GPS 1126088704,1128669184. GW170814 is a confident detection and was searched to display the correctness of our algorithm as shown in Figure 5.11c. The two other searches were neither confident detections nor marginal triggers[4] as described in the GWTC-1 catalogue [29]. The scale for the plot depends on the length of data segment used, for instance, 5.11a is a data segment of 65535 samples. Majority of the results show no presence of a signal, as one would expect. Interestingly though, one of the BP analysis (for GPS 1126088704) results in a tiny spike shown in Figure 5.11a. This might be potentially a GW and would require further investigation.

[3]File from Livingston detector, for say GPS(1128670422). Each file consisting of 4096 seconds of strain data sampled at 4kHz.

[4]false alarm rate less than 1 per 30 days

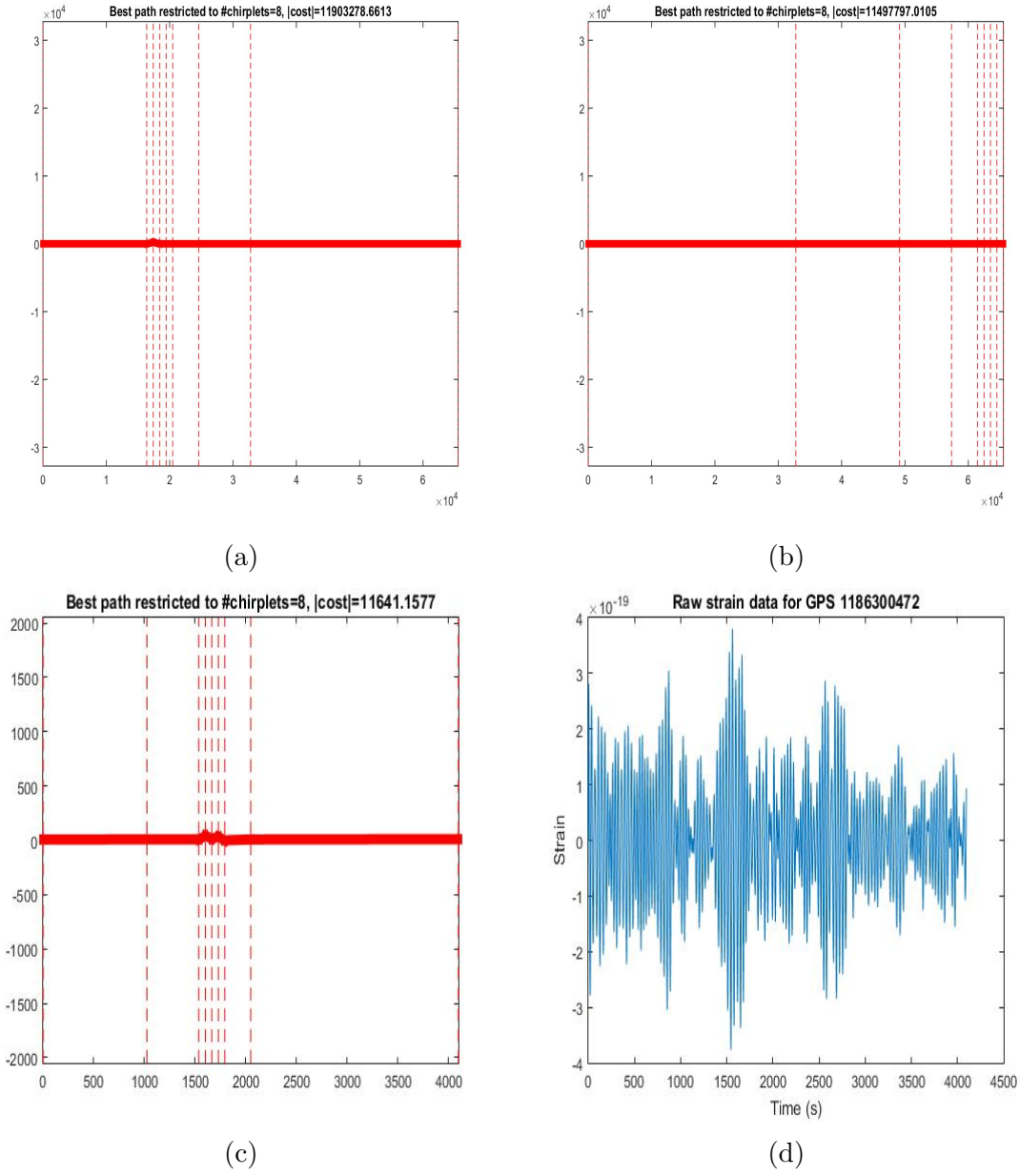

Figure 5.11: Best path plots are shown for 3 different segments of real data using 8 multiscale chirplets. X-axis represents time in number of samples (s*Fs), Y-axis represents the Frequency (Hz). a) GPS 1126088704 b) 1128669184 c) 1186300472 or GW170809 is a confident detection in GWTC-1 catalogue d) Sample strain data of full 4096 seconds.

5.5 Summary of the chapter

The aim of this thesis was to provide proof of concept for ppE and showcase the practical potential for the same. The ppE waveforms (templates) when used with matched filtering on detected potential signals, can be tested for the signal's deviation from General Relativity. The results shown in this chapter affirms the efficiency of ChirpLab and provides evidence for the possibility of non-GR waves interpreted as GR waves. We, first, show simulated GR waveforms with currently used approximants for the purpose of validating our computation method. It also helps the reader (new to the field) to visualize CBC inspiral waveforms. Our extended ChirpLab is modeled with ppE waveforms for two theories, Brans-Dicke and Massive gravity. We use different values of β for the generation of the waveforms. We find that the β_{BD} varies more linearly as compared to β_{MG}, implying that MG waveform will converge to GR before BD waveform does. These generated ppE waveforms are to put to test through ChirpLab's BP detection algorithm. This serves two purposes:

- Illustrates the subtlity between GR and non-GR waves. Henceforth proving the possible deviations introduced in the parameter estimation of non-GR signals with GR templates.
- Displays the robustness of non-template based ChirpLab detection method for all types of gravitational waves.

The BP statistics for ppE waveform shows presence of a GW for both the theories implemented (BD and MG). For MG signal, the chirplets (divided by the vertical dashes) are closer to the *spike*, whereas for BD signal the chirplets are spread out during the last few seconds of the inspiral. Lastly, the results from our open search is shown. We scan real aLIGO data for any undiscovered signal. One of our BP plots shows significant *spike* to be considered as coincidental noise. Further investigation for the potential GW data segment will be required.

Chapter 6

Concluding remarks

6.1 Conclusion

The motivation for the thesis was to obtain proof of concept for the analysis of GWs independent of theoretical assumptions. The approaches considered here are exploratory and will need to be refined. Nevertheless, these approaches demonstrate the need and effectiveness of taking what Pretorius and Yunes call the 'theoretical bias' of the current models into account. Moreover, their (Pretorius and Yunes) viewpoint can be used for constructing post-data analysis to probe the data from multiple perspectives. We used a generalized non-template based detection software ChirpLab along side ppE waveforms to display a new aspect for the post-data analysis.

A statistical approach, like Best Path statistic, is effective for the detection of gravitational waves. BP statistic also illustrates the robustness with no significant false negative in the presence of non-GR waveforms. The BP detection method seems promising with non-template based searches for real data as shown in Section 5.4. Best path statistic seems promising with this new set of radiation waves.

Furthermore, as seen in Section 5.2.2, competing theories vary ever so slightly in the simulated waveforms. This can potentially affect parameter estimation when done using template banks generated by approximations like PN theory and EOB formalism. Investigating the effects of parameter estimation will be the next step for this research project.

6.2 Future work

This project only focused on the Inspiral phase, as the modeling for merger-ringdown would be out of scope for this thesis. The next step would be to include the full IMR waveform for ppE testing. Also, the same approach can be incorporated in C source code for `lalsuite` to implement ppE testing.

Another advancement would be to incorporate a parameter estimation method that allows for unexpected behavior of GWs. Thus, giving rise to a new pipeline for analysis of GWs independent of theoretical assumptions. Specially for burst and stochastic GWs where researchers are expecting the unexpected.

Recent gravitational wave detection has hardly scratched the surface with gravitational wave astronomy. As was with the discovery of EM waves, we do not know what is in store for GWs maybe we will have devices in the future utilizing GWs. There will definitely be revelations about space, time, and potentially, the very start of this story the Big Bang.

Bibliography

[1] About "aLIGO", August 2017. URL https://www.ligo.caltech.edu/page/about-aligo.

[2] GW Open Science Center, August 2017. URL https://www.gw-openscience.org/catalog/GWTC-1-confident/html/.

[3] LIGO Scientific Collaboration - The science of LSC research, August 2017. URL https://www.ligo.org/science/GW-Burst.php.

[4] LIGO Hanford, August 2017. URL https://www.ligo.caltech.edu/image/ligo20150731f.

[5] LIGO | Livingston, August 2017. URL https://www.ligo.caltech.edu/LA#.

[6] LIGO's Interferometer, August 2017. URL https://www.ligo.caltech.edu/page/ligos-ifo.

[7] Sources and Types of Gravitational Waves, August 2017. URL https://www.ligo.caltech.edu/page/gw-sources.

[8] Timeline, August 2017. URL https://www.ligo.caltech.edu/page/timeline.

[9] Core package to analyze gravitational-wave data, find signals, and study their parameters. This package was used in the first direct detection of gravitational waves (GW150914), and is used in the .., June 2019. URL https://github.com/gwastro/pycbc. original-date: 2015-03-03T12:19:19Z.

[10] B. P. Abbott, R. Abbott, T. D. Abbott, M. R. Abernathy, J. S. Areeda, N. Arnaud, Z. Zhou, X. J. Zhu, M. E. Zucker, S. E. Zuraw, J. Zweizig, and et al LIGO Scientific Collaboration and Virgo Collaboration. Observation of Gravitational Waves from a Binary Black Hole Merger. *Physical Review Letters*, 116 (6), February 2016. ISSN 0031-9007, 1079-7114. doi: 10.1103/PhysRevLett.116.061102. URL https://link.aps.org/doi/10.1103/PhysRevLett.116.061102.

[11] P. Ajith, S. Babak, Y. Chen, M. Hewitson, B. Krishnan, J. T. Whelan, B. Bruegmann, P. Diener, J. Gonzalez, M. Hannam, S. Husa, M. Koppitz, D. Pollney, L. Rezzolla, L. Santamaria, A. M. Sintes, U. Sperhake, and J. Thornburg. Phenomenological template family for black-hole coalescence waveforms. *Classical and Quantum Gravity*, 24(19):S689–S699, October 2007. ISSN 0264-9381, 1361-6382. doi: 10.1088/0264-9381/24/19/S31. URL http://arxiv.org/abs/0704.3764. arXiv: 0704.3764.

[12] P. Ajith, M. Hannam, S. Husa, Y. Chen, B. Bruegmann, N. Dorband, D. Mueller, F. Ohme, D. Pollney, C. Reisswig, L. Santamaria, and J. Seiler. Inspiral-merger-ringdown waveforms for black-hole binaries with non-precessing spins. *Physical Review Letters*, 106(24):241101, June 2011. ISSN 0031-9007, 1079-7114. doi: 10.1103/PhysRevLett.106.241101. URL http://arxiv.org/abs/0909.2867. arXiv: 0909.2867.

[13] Stephon Alexander and Nicolas Yunes. Chern-Simons Modified General Relativity. *Physics Reports*, 480(1-2):1–55, August 2009. ISSN 03701573. doi: 10.1016/j.physrep.2009.07.002. URL http://arxiv.org/abs/0907.2562. arXiv: 0907.2562.

[14] Warren G. Anderson and R. Balasubramanian. Time-frequency detection of Gravitational Waves. *Physical Review D*, 60(10):102001, October 1999. ISSN 0556-2821, 1089-4918. doi: 10.1103/PhysRevD.60.102001. URL http://arxiv.org/abs/gr-qc/9905023. arXiv: gr-qc/9905023.

[15] Hideki Asada and Toshifumi Futamase. Chapter 2. Post-Newtonian ApproximationIts Foundation and Applications. *Progress of Theoretical Physics Supplement*, 128:123–181, March 1997. ISSN 0375-9687. doi: 10.1143/PTPS.128.123. URL https://academic.oup.com/ptps/article/doi/10.1143/PTPS.128.123/1930024.

[16] Estelle Asmodelle. Tests of General Relativity: A Review. *arXiv:1705.04397 [gr-qc]*, May 2017. URL http://arxiv.org/abs/1705.04397. arXiv: 1705.04397.

[17] Jacob D. Bekenstein. Relativistic gravitation theory for the MOND paradigm. *Physical Review D*,

71(6):069901, March 2005. ISSN 1550-7998, 1550-2368. doi: 10.1103/PhysRevD.71.069901. URL http://arxiv.org/abs/astro-ph/0403694. arXiv: astro-ph/0403694.

[18] Jacob D. Bekenstein. Tensor-vector-scalar-modified gravity: from small scale to cosmology. *Philosophical Transactions of the Royal Society A: Mathematical, Physical and Engineering Sciences*, 369 (1957):5003–5017, December 2011. ISSN 1364-503X, 1471-2962. doi: 10.1098/rsta.2011.0282. URL http://arxiv.org/abs/1201.2759. arXiv: 1201.2759.

[19] Emanuele Berti, Enrico Barausse, Vitor Cardoso, Leonardo Gualtieri, Paolo Pani, Hajime Sotani, and et al Zilhao, Miguel. Testing General Relativity with Present and Future Astrophysical Observations. *Classical and Quantum Gravity*, 32(24):243001, December 2015. ISSN 0264-9381, 1361-6382. doi: 10.1088/0264-9381/32/24/243001. URL http://arxiv.org/abs/1501.07274. arXiv: 1501.07274.

[20] Luc Blanchet. Post-Newtonian Theory and its Application. page 16.

[21] Luc Blanchet, Bala R. Iyer, Clifford M. Will, and Alan G. Wiseman. Gravitational waveforms from inspiralling compact binaries to second-post-Newtonian order. *Classical and Quantum Gravity*, 13(4): 575–584, April 1996. ISSN 0264-9381, 1361-6382. doi: 10.1088/0264-9381/13/4/002. URL http://arxiv.org/abs/gr-qc/9602024. arXiv: gr-qc/9602024.

[22] C. Brans and R. H. Dicke. Mach's Principle and a Relativistic Theory of Gravitation. *Physical Review*, 124(3):925–935, November 1961. doi: 10.1103/PhysRev.124.925. URL https://link.aps.org/doi/10.1103/PhysRev.124.925.

[23] A. Buonanno and T. Damour. Effective one-body approach to general relativistic two-body dynamics. November 1998. doi: 10.1103/PhysRevD.59.084006. URL https://arxiv.org/abs/gr-qc/9811091v1.

[24] Emmanuel Candes. ChirpLab 1.1: User's Guide. URL https://www.academia.edu/2846994/ChirpLab_1.1_User_s_Guide.

[25] Emmanuel J. Candes, Philip R. Charlton, and Hannes Helgason. Detecting Highly Oscillatory Signals by Chirplet Path Pursuit. *arXiv:gr-qc/0604017*, April 2006. URL http://arxiv.org/abs/gr-qc/0604017. arXiv: gr-qc/0604017.

[26] S. Chandrasekhar. The Post-Newtonian Effects of General Relativity on the Equilibrium of Uniformly Rotating Bodies. I. The Maclaurin Spheroids and the Virial Theorem. URL https://www.researchgate.net/publication/234556087_The_Post-Newtonian_Effects_of_General_Relativity_on_the_Equilibrium_of_Uniformly_Rotating_Bodies_I_The_Maclaurin_Spheroids_and_the_Virial_Theorem.

[27] S. Chandrasekhar. Post-Newtonian Equations of Hydrodynamics and the Stability of Gaseous Masses in General Relativity. *Physical Review Letters*, 14(8):241–244, February 1965. ISSN 0031-9007. doi: 10.1103/PhysRevLett.14.241. URL https://link.aps.org/doi/10.1103/PhysRevLett.14.241.

[28] Éric Chassande-Mottin, Archana Pai, and Olivier Rabaste. Chains of chirplets for the detection of gravitational wave chirps. In *Wavelets XII*, volume 6701, page 670112. International Society for Optics and Photonics, September 2007. doi: 10.1117/12.733966. URL https://www.spiedigitallibrary.org/conference-proceedings-of-spie/6701/670112/Chains-of-chirplets-for-the-detection-of-gravitational-wave-chirps/10.1117/12.733966.short.

[29] The LIGO Scientific Collaboration, the Virgo Collaboration, B. P. Abbott, R. Abbott, T. D. Abbott, S. Abraham, F. Acernese, K. Ackley, M. E. Adams, Zucker, and et al Zweizig, J. GWTC-1: A Gravitational-Wave Transient Catalog of Compact Binary Mergers Observed by LIGO and Virgo during the First and Second Observing Runs. *arXiv:1811.12907 [astro-ph, physics:gr-qc]*, November 2018. URL http://arxiv.org/abs/1811.12907. arXiv: 1811.12907.

[30] Thibault Damour and Alessandro Nagar. The Effective One Body description of the Two-Body problem. *arXiv:0906.1769 [gr-qc]*, June 2009. URL http://arxiv.org/abs/0906.1769. arXiv: 0906.1769.

[31] Ray d'Inverno. *Introducing Einstein's Relativity*. Oxford University Press, Oxford, New York, August 1992. ISBN 978-0-19-859653-0.

[32] David L. Donoho and Xiaoming Huo. Beamlets and Multiscale Image Analysis. In Timothy J. Barth, Tony Chan, and Robert Haimes, editors, *Multiscale and Multiresolution Methods*, Lecture Notes in Computational Science and Engineering, pages 149–196. Springer Berlin Heidelberg, 2002. ISBN 978-3-642-56205-1.

[33] C. Eling, T. Jacobson, and D. Mattingly. Einstein-Aether Theory. *arXiv:gr-qc/0410001*, September 2004. URL http://arxiv.org/abs/gr-qc/0410001. arXiv: gr-qc/0410001.

[34] Christopher Eling. Energy in the Einstein-Aether Theory. *Physical Review D*, 80(12):129905, December 2009. ISSN 1550-7998, 1550-2368. doi: 10.1103/PhysRevD.80.129905. URL http://arxiv.org/abs/gr-qc/0507059. arXiv: gr-qc/0507059.

[35] M. Gasperini. Singularity prevention and broken Lorentz symmetry. *Classical and Quantum Gravity*, 4 (2):485–494, March 1987. ISSN 0264-9381. doi: 10.1088/0264-9381/4/2/026. URL https://doi.org/10.1088%2F0264-9381%2F4%2F2%2F026.

[36] Giles Hammond, Stefan Hild, and Matthew Pitkin. Advanced technologies for future laser-interferometric gravitational wave detectors. *Journal of Modern Optics*, 61, February 2014. doi: 10.1080/09500340.2014.920934.

[37] Mark Hannam, Patricia Schmidt, Alejandro Bohé, Leila Haegel, Sascha Husa, Frank Ohme, Geraint Pratten, and Michael Pürrer. A simple model of complete precessing black-hole-binary gravitational waveforms. August 2013. doi: 10.1103/PhysRevLett.113.151101. URL https://arxiv.org/abs/1308.3271v2.

[38] Mike Hockney. *The Last Man Who Knew Everything*. Lulu Press, Inc, July 2013. ISBN 978-1-291-50469-9. Google-Books-ID: 7mQnDAAAQBAJ.

[39] Russell A. Hulse. The discovery of the binary pulsar. *Reviews of Modern Physics*, 66(3):699–710, July 1994. ISSN 0034-6861, 1539-0756. doi: 10.1103/RevModPhys.66.699. URL https://link.aps.org/doi/10.1103/RevModPhys.66.699.

[40] E J. Howell, Antonia Rowlinson, D M. Coward, P D. Lasky, David Kaplan, E Thrane, G Rowell, Duncan Galloway, Fang Yuan, Richard Dodson, T Murphy, G C. Hill, Igor Andreoni, L Spitler, and Anthony Horton. Hunting Gravitational Waves with Multi-Messenger Counterparts: Australia's Role. *Publications of the Astronomical Society of Australia*, 32, November 2015. doi: 10.1017/pasa.2015.49.

[41] Daniel J. Kennefick. *No Shadow of a Doubt: The 1919 Eclipse That Confirmed Einstein's Theory of Relativity*. Princeton University Press, April 2019. ISBN 978-0-691-19005-1. Google-Books-ID: N_p1DwAAQBAJ.

[42] Sebastian Khan, Sascha Husa, Mark Hannam, Frank Ohme, Michael Pürrer, Xisco Jiménez Forteza, and Alejandro Bohé. Frequency-domain gravitational waves from non-precessing black-hole binaries. II. A phenomenological model for the advanced detector era. *Physical Review D*, 93(4), February 2016. ISSN 2470-0010, 2470-0029. doi: 10.1103/PhysRevD.93.044007. URL http://arxiv.org/abs/1508.07253. arXiv: 1508.07253.

[43] Sebastian Khan, Katerina Chatziioannou, Mark Hannam, and Frank Ohme. Phenomenological model for the gravitational-wave signal from precessing binary black holes with two-spin effects. *arXiv:1809.10113 [gr-qc]*, September 2018. URL http://arxiv.org/abs/1809.10113. arXiv: 1809.10113.

[44] Luis Lehner. Numerical Relativity: A review. *Classical and Quantum Gravity*, 18(17):R25–R86, September 2001. ISSN 0264-9381, 1361-6382. doi: 10.1088/0264-9381/18/17/202. URL http://arxiv.org/abs/gr-qc/0106072. arXiv: gr-qc/0106072.

[45] Tjonnie G F Li. Extracting Physics from Gravitational Waves. *Extracting Physics from Gravitational Waves*, page 256.

[46] LIGO. Simulated continuous gw, August 2017. URL https://www.black-holes.org/sound/Periodic.wav.

[47] Michele Maggiore. *Gravitational Waves: Volume 1: Theory and Experiments*. Oxford University Press, October 2007. ISBN 978-0-19-171766-6. URL https://www-oxfordscholarship-com.ezproxy.lib.vt.edu/view/10.1093/acprof:oso/9780198570745.001.0001/acprof-9780198570745.

[48] Deborah Mayo. Error and the Growth of Experimental Knowledge. *International Studies in the Philosophy of Science*, 15(1):455–459, 1996.

[49] C. W. Misner, K. S. Thorne, and J.A. Wheeler. *Gravitation*. 2nd edition, 2017. URL https://press.princeton.edu/titles/11169.html.

[50] Fahad Nasir. Simulation of Gravitational Waves and Binary Black Holes Space-times. page 70.

[51] Benjamin J. Owen and B. S. Sathyaprakash. Matched filtering of gravitational waves from inspiraling compact binaries: Computational cost and template placement. *Physical Review D*, 60(2):022002, June 1999. ISSN 0556-2821, 1089-4918. doi: 10.1103/PhysRevD.60.022002. URL http://arxiv.org/abs/gr-qc/9808076. arXiv: gr-qc/9808076.

[52] Yi Pan, Alessandra Buonanno, Andrea Taracchini, Lawrence E. Kidder, Abdul H. Mroué, Harald P. Pfeiffer, Mark A. Scheel, and Béla Szilágyi. Inspiral-merger-ringdown waveforms of spinning, precessing black-hole binaries in the effective-one-body formalism. *Physical Review D*, 89(8):084006, April 2014. doi: 10.1103/PhysRevD.89.084006. URL https://link.aps.org/doi/10.1103/PhysRevD.89.084006.

[53] Peter Saulson. *Fundamentals of Interferometric gravitational wave detectors*. World scientific publishing Co. Pte. Ltd. ISBN 978-981-02-1820-1.

[54] Karl Popper. *Conjectures and Refutations: The Growth of Scientific Knowledge*. Routledge, 1962.

[55] Karl R. Popper. *The Logic of Scientific Discovery*. Routledge, 1959.

[56] R. V. Pound and G. A. Rebka. Gravitational Red-Shift in Nuclear Resonance. *Physical Review Letters*, 3(9):439–441, November 1959. doi: 10.1103/PhysRevLett.3.439. URL https://link.aps.org/doi/10.1103/PhysRevLett.3.439.

[57] Bernhard Rothenstein and Stefan Popescu. Lorentz transformation, time dilation, length contraction and Doppler Effect - all at once. page 9.

[58] R. H. Sanders. A tensor-vector-scalar framework for modified dynamics and cosmic dark matter. *Monthly Notices of the Royal Astronomical Society*, 363(2):459–468, October 2005. ISSN 0035-8711, 1365-2966. doi: 10.1111/j.1365-2966.2005.09375.x. URL http://arxiv.org/abs/astro-ph/0502222. arXiv: astro-ph/0502222.

[59] L. Santamaria, F. Ohme, P. Ajith, B. Bruegmann, N. Dorband, M. Hannam, S. Husa, P. Moesta, D. Pollney, C. Reisswig, E. L. Robinson, J. Seiler, and B. Krishnan. Matching post-Newtonian and numerical relativity waveforms: systematic errors and a new phenomenological model for non-precessing black hole binaries. *Physical Review D*, 82(6):064016, September 2010. ISSN 1550-7998, 1550-2368. doi: 10.1103/PhysRevD.82.064016. URL http://arxiv.org/abs/1005.3306. arXiv: 1005.3306.

[60] Teviet Creighton and Bruce Allen. GRASP Routines: Template Bank Generation and Searching, 1997. URL https://dcc.ligo.org/public/0028/T970256/000/T970256-01.pdf.

[61] Kip S. Thorne. *The Science of Interstellar*. November 2014.

[62] Kip S. Thorne and Clifford M. Will. Theoretical Frameworks for Testing Relativistic Gravity. I. Foundations. *The Astrophysical Journal*, 163:595, February 1971. ISSN 0004-637X, 1538-4357. doi: 10.1086/150803. URL http://adsabs.harvard.edu/doi/10.1086/150803.

[63] Samantha A. Usman, Alexander H. Nitz, Ian W. Harry, Christopher M. Biwer, Duncan A. Brown, Miriam Cabero, Collin D. Capano, Tito Dal Canton, Thomas Dent, Stephen Fairhurst, Marcel S.

Kehl, Drew Keppel, Badri Krishnan, Amber Lenon, Andrew Lundgren, Alex B. Nielsen, Larne P. Pekowsky, Harald P. Pfeiffer, Peter R. Saulson, Matthew West, and Joshua L. Willis. The PyCBC search for gravitational waves from compact binary coalescence. *Classical and Quantum Gravity*, 33 (21):215004, November 2016. ISSN 0264-9381, 1361-6382. doi: 10.1088/0264-9381/33/21/215004. URL http://arxiv.org/abs/1508.02357. arXiv: 1508.02357.

[64] M. Vaughan. *The Fabry-Perot Interferometer : History, Theory, Practice and Applications*. Routledge, November 2017. ISBN 978-1-351-41051-9. doi: 10.1201/9780203736715. URL https://www.taylorfrancis.com/books/9781351410519.

[65] Clifford M. Will. Theoretical Frameworks for Testing Relativistic Gravity. III. Conservation Laws, Lorentz Invariance, and Values of the PPN Parameters. *The Astrophysical Journal*, 169:125, October 1971. doi: 10.1086/151124. URL https://ui.adsabs.harvard.edu/#abs/1971ApJ...169..125W/abstract.

[66] Clifford M. Will. On the unreasonable effectiveness of the post-Newtonian approximation in gravitational physics. *Proceedings of the National Academy of Sciences*, 108(15):5938–5945, April 2011. ISSN 0027-8424, 1091-6490. doi: 10.1073/pnas.1103127108. URL http://arxiv.org/abs/1102.5192. arXiv: 1102.5192.

[67] Clifford M. Will. The Confrontation between General Relativity and Experiment. *Living Reviews in Relativity*, 17(1), December 2014. ISSN 2367-3613, 1433-8351. doi: 10.12942/lrr-2014-4. URL http://arxiv.org/abs/1403.7377. arXiv: 1403.7377.

[68] Clifford M. Will and Helmut W. Zaglauer. Gravitational radiation, close binary systems, and the Brans-Dicke theory of gravity. *The Astrophysical Journal*, 346:366–377, November 1989. ISSN 0004-637X. doi: 10.1086/168016. URL http://adsabs.harvard.edu/abs/1989ApJ...346..366W.

[69] Nicolas Yunes and Frans Pretorius. Fundamental Theoretical Bias in Gravitational Wave Astrophysics and the Parameterized Post-Einsteinian Framework. *Physical Review D*, 80(12), December 2009. ISSN

1550-7998, 1550-2368. doi: 10.1103/PhysRevD.80.122003. URL http://arxiv.org/abs/0909.3328. arXiv: 0909.3328.

[70] Nicolás Yunes and Frans Pretorius. Dynamical Chern-Simons modified gravity: Spinning black holes in the slow-rotation approximation. *Physical Review D*, 79(8):084043, April 2009. doi: 10.1103/PhysRevD.79.084043. URL https://link.aps.org/doi/10.1103/PhysRevD.79.084043.

Appendices

Appendix A

Description of $\tilde{h}_{gr}(f)$

This appendix describes the equations used to compute simulated waveforms and hence the templates generated using ppE. All equations follow,

$$M_{\odot} = 1.98 \times 10^{30} kg \quad \text{(Mass of Sun)}$$

$$m_{tot} = m1 + m2 \quad \text{(Total mass of binary)}$$

$$\text{where,} \quad m1, m2 = 1.4 M_{\odot} \quad \text{(Individual masses)}$$

$$\eta = \frac{m1 \times m2}{m_{tot}^2} \quad \text{(Symmetric mass ratio)}$$

$$M_{chirp} = \eta^{3/5} \times m_{tot} \quad \text{(Chirp mass/Radiated mass)}$$

$$t_c \quad \text{(Time of coalescence)} \quad t \quad \text{(instantaneous time)}$$

$$T_0 = 4.92 \times 10^{-6} sec \quad \text{(Solar time)}$$

The phase as a function of time is given as,

$$\phi(t) = \frac{-2}{\eta}\theta^{-5}\big(1 + (\frac{3715}{8064} + \frac{55}{96}\eta)\theta^2 + (-3\pi/4)\theta^3 + (\frac{9275495}{14450688} + \frac{284875}{258048}\eta + \frac{1855}{2048}\eta^2)\theta^4\big) \tag{A.1}$$

where θ is,

$$\theta = \frac{\eta(t_c - t)}{5 m_{tot} T_0}\big)^{-1/8} \tag{A.2}$$

The orbital frequency as a function of time,

$$
\begin{aligned}
f(t) = \frac{\theta^3}{8\pi m_{tot} T_0}\big(1 + (\frac{743}{2688} + \frac{11}{32}\eta)\theta^2 + (-3\pi/10)\theta^3 + (\frac{1855099}{14450688} \\
+ \frac{56975}{258048}\eta + \frac{371}{2048}\eta^2)\theta^4 + ((\frac{7729}{21504} - \frac{13}{256}\eta)\pi)\theta^5 \\
+ (\frac{720817631400877}{288412611379200} + \frac{53}{200}\pi^2 + \frac{107}{280}\gamma + (\frac{25302017977}{4161798144} - \frac{451}{2048}\pi^2)\eta \\
- \frac{30913}{1835008}\eta^2 + \frac{235925}{1769472}\eta^3 + \frac{107}{280}log(2\theta))\theta^6 \\
+ ((\frac{-188516689}{433520640} - \frac{-97765}{258048}\eta + \frac{141769}{1290240}\eta^2)\pi)\theta^7\big)
\end{aligned}
\tag{A.3}
$$

Velocity v(t) is found as roots of the following (A.4), time as a function of velocity.

$$
\begin{aligned}
t(v) &= t_c + m_{tot}\int_v^{v_o} \frac{E(v)}{F(v)} \\
&= t_c - \frac{5 m_{tot} T_0}{(256\eta)v^{-8}}\big(1 + (\frac{743}{252} + \frac{11}{3}\eta)v^2 + (-32\pi/5)v^3 + (\frac{3058673}{508032} \\
&+ \frac{5429}{504}\eta + \frac{617}{72}\eta^2)v^4 + ((\frac{7729}{252} - \frac{13}{3}\eta)\pi)v^5 \\
&+ (\frac{-10052469856691}{23471078400} + \frac{128}{3}\pi^2 + \frac{6848}{105}\gamma + (\frac{31477553127}{3048192} - \frac{451}{12}\pi^2)\eta \\
&- \frac{15211}{1728}\eta^2 + \frac{25565}{1296}\eta^3 + \frac{3424}{105}log(16v^2))v^6 \\
&+ ((\frac{-15419335}{127008} - \frac{75703}{756}\eta + \frac{14809}{378}\eta^2)\pi)v^7\big)
\end{aligned}
\tag{A.4}
$$

Hence, we get the full waveform in terms of velocity as:

$$
h_{gr}(t) = v^2(t) cos(2\phi(t)) \tag{A.5}
$$

The Fourier transformation of Equation A.5 gives $\tilde{h}_{gr}(f)$. The ppE formalism adds a correction term to $\tilde{h}_{gr}(f)$ for inspiral phase as described by Equation (3.5).